Spatiotemporal dynamics of maximal and minimal EEG spectral power

Melisa Menceloglu, Marcia Grabowecky, & Satoru Suzuki
Northwestern university, Evanston, IL, U.S.A.

Send correspondences to:
Satoru Suzuki
Northwestern University
Department of Psychology
Interdepartmental Neuroscience
2029 Sheridan Road, Evanston, IL 60208
Phone: (847)467-1271
Email: satoru@northwestern.edu

Abstract

Oscillatory neural activities are prevalent in the brain with their phase realignment contributing to the coordination of neural communication. Phase realignments would have especially strong (or weak) impact when neural activities are strongly synchronized (or desynchronized) within the interacting sub-populations. We report that the spatiotemporal dynamics of strong regional synchronization (reflected in maximal EEG spectral power)—*activation*—and strong regional desynchronization (reflected in minimal EEG spectral power)—*suppression*—are characterized by the spatial segregation of isolated small-scale networks and highly cooperative large-scale networks. Specifically, small-scale spectral-power activations and suppressions involving only 2%–7% of EEG scalp sites were prolonged (relative to stochastic dynamics) and consistently co-localized in a frequency specific manner. For example, the small-scale networks for θ, α, β_1, and β_2 bands (4–30 Hz) consistently included frontal sites when the eyes were closed, whereas the small-scale network for γ band (31–55 Hz) consistently clustered in medial-central-posterior sites whether the eyes were open or closed. Large-scale activations and suppressions involving over 30% of EEG sites were also prolonged and generally clustered in regions complementary to where small-scale activations and suppressions clustered. In contrast, intermediate-scale activations and suppressions tended to follow stochastic dynamics and were less consistently localized. These results suggest that strong synchronizations and desynchronizations occur in small-scale and large-scale networks that are spatially segregated and frequency specific. These synchronization networks may broadly segregate the relatively independent and highly cooperative oscillatory processes while phase realignments fine-tune the network configurations based on behavioral demands.

Introduction

Many studies have investigated the dynamics of macroscopic-level oscillatory neural activity in humans by examining the spatiotemporal patterns of spectral-power, phase, and phase-amplitude relations within and across frequency bands and brain regions using EEG/MEG methods. Those studies characterized network features such as modules, hubs, and motifs based on the spatial organizations of amplitude relations, phase relations, and information transfer [1–8; see 9 for a review]. This line of investigation has revealed frequency-specific hierarchical networks (including networks and sub-networks) whose structures and activities correlate with a variety of behavioral functions [10–22] and mental states [23–26]. While prior studies examined intricate amplitude, phase, and phase-amplitude relations underlying specific behavioral functions and mental states, we have focused on identifying general rules governing the spontaneous spatiotemporal dynamics of EEG and EEG spectral-power activity [27, 39–40].

Neural communications are facilitated when the phases of oscillating neural excitability are aligned between sub-populations (taking into account conduction delays). Temporary networks are established by aligning the phases of oscillatory neural activity among appropriate groups of sub-populations to facilitate task-specific neural communications (see citations above). Different networks are engaged or disengaged as the phases of oscillations of different frequency bands are aligned or misaligned across different groups of sub-populations. Such phase adjustments would have an especially strong (or weak) impact on neural interactions when the oscillatory activities within the relevant sub-populations are strongly synchronized (or desynchronized). Thus, the strength and configuration of temporary networks established through phase alignments are constrained by which sub-populations are concurrently strongly synchronized or desynchronized.

We hypothesized that sub-populations in different brain regions may differ in their tendencies to strongly synchronize concurrently with other sub-populations. Some sub-populations may tend to strongly synchronize independently of other sub-populations, tending to carry on relatively isolated processes, whereas some sub-populations may tend to strongly synchronize concurrently with many other sub-populations, tending to participate in large-scale phase-dependent networks. We sought to identify these regional synchronization networks as they would impose substantial spatiotemporal constraints on the temporary networks established through phase realignments.

We assumed that the degree of oscillatory synchronization within a neural sub-population was proportional to the spectral power of surface-Laplacian transformed EEG obtained at a corresponding scalp site (at the spatial resolution of 1–2 cm; see Methods). We thresholded spectral power (see Results) to examine the spatiotemporal dynamics of maximal and minimal spectral-power activity at each site, which we respectively refer to as "activation" and "suppression," reflective of strong within-sub-population synchronization (a large number of neurons synchronously oscillating) and desynchronization (only a small number of neurons synchronously oscillating or a sizable number of neurons incoherently oscillating).

Spectral-power activations and suppressions may occur in relative isolation (concurrently occurring at only a few sites), in moderately distributed regions, or in widespread regions (concurrently occurring at a large number of sites) at different moments. Our results provide converging evidence suggesting that isolated and widespread spectral-power activations and suppressions are actively maintained and distinctly co-localized in a frequency specific manner, segregating the sub-populations primarily engaged in relatively independent processes (often co-synchronized or co-desynchronized with only 2%–7% of sites) and those primarily engaged in highly cooperative processes (often co-synchronized or co-desynchronized with over 30% of sites).

Methods

Participants.

Fifty-two Northwestern University students (35 women, 1 non-binary; ages 18 to 29 years, *M* = 20.75, *SD* = 2.52) gave informed consent to participate for monetary compensation ($10/hr). All were right-handed, had normal hearing and normal or corrected-to-normal vision, and had no history of concussion. They were tested individually in a dimly lit or dark room. The study protocol was approved by the Northwestern University Institutional Review Board. Participants p1–p7 and p12–p28 (*N* = 24) participated in a rest-with-eyes-closed condition in which EEG was recorded for ~5 min while participants rested with their eyes closed and freely engaged in spontaneous thoughts. Participants p8–p28 (*N* = 21) additionally participated in a silent-nature-video condition in which EEG was recorded for ~5 min while they viewed a silent nature video. To evaluate test-retest reliability, the silent-nature-video condition was run twice (20-30 min apart), labeled as earlier viewing and later viewing in the analyses. A generic nature video was presented on a 13-inch, 2017 MacBook Pro, 2880(H)-by-1800(V)-pixel-resolution LCD monitor with normal brightness and contrast settings, placed 100 cm away from participants, subtending

approximately 16°(H)-by-10°(V) of visual angle. Participants p29–p52 (*N* = 24) participated in the replication of the rest-with-the-eyes-closed condition and a rest-with-eyes-open-in-dark condition which was the same as the former except that the room was darkened and participants kept their eyes open while blinking naturally. These EEG data were previously analyzed for a different purpose [27].

EEG recording and pre-processing.

While participants rested with their eyes closed, rested with their eyes open in dark, or viewed a silent nature video for approximately 5 min, EEG was recorded from 60 scalp electrodes (although we used a 64-electrode montage, we excluded signals from noise-prone electrodes, *Fpz*, *Iz*, *T9*, and *T10*) at a sampling rate of 512 Hz using a BioSemi ActiveTwo system (see www.biosemi.com for details). Electrooculographic (EOG) activity was monitored using four face electrodes, one placed lateral to each eye and one placed beneath each eye. Two additional electrodes were placed on the left and right mastoid area. The EEG data were preprocessed using EEGLAB and ERPLAB toolboxes for MATLAB [28–29]. The data were re-referenced offline to the average of the two mastoid electrodes, bandpass-filtered at 0.01–80 Hz, and notch-filtered at 60 Hz (to remove power-line noise that affected the EEG signals from some participants). For the EEG signals recorded while participants rested with their eyes open in the dark or while they viewed a silent nature video, an Independent Component Analysis (ICA) was conducted using EEGLABs' *runica* function [30–31] to remove components reflecting blinks. To reduce effects of volume conduction (to approximately within adjacent sites; e.g., [32]), to virtually eliminate the effects of reference electrode choice (verified), as well as to facilitate data-driven determinations of EEG current sources, we applied the surface-Laplacian transform to all EEG signals [33–35] using the Perrin and colleagues' method [36–38] with a typical set of parameter values [32]. We refer to the surface-Laplacian transformed EEG signals representing the current-source activity across the 60 scalp sites simply as EEG signals. These EEG-recording and pre-processing procedures were identical to those used in our prior study [27].

EEG analysis.

To focus on oscillatory neural activity, we used the temporal derivative of EEG (macroscopically estimating the underlying electrical currents) that virtually eliminated the non-oscillatory $1/f^{\beta}$ spectral backgrounds [27, 39–40] without having to estimate and discount them in sliding-time windows. We generated phase-scrambled controls whose spectral power

fluctuated stochastically (i.e., unpredictably in a memory-free manner) while maintaining the time-averaged spectral-amplitude profiles of the actual EEG data. While phase-scrambling can be performed using several different methods, we chose discrete cosine transform, DCT [41]. In short, we transformed each ~5 min EEG waveform with type-2 DCT, randomly shuffled the signs of the coefficients, and then inverse-transformed it with type-3 DCT (the "inverse DCT"), which yielded a phase-scrambled version. DCT phase-scrambling is similar to DFT (discrete Fourier transform) phase-scrambling except that it is less susceptible to edge effects. We previously verified that DCT phase-scrambling generated waveforms whose spectral-power fluctuations conformed to exponential distributions indicative of a Poisson point process (a stochastic process), with little to no distortion to the time-averaged spectral-amplitude profiles of EEG [27].

To investigate how spectral power (amplitude squared) fluctuated, we used a Morlet wavelet-convolution method [32] to extract spectral amplitudes as a function of time. We decomposed each EEG waveform (i.e., its temporal derivative) into a time series of spectral power using Morlet wavelets with 200 center frequencies, f_c's, between 3 Hz and 60 Hz. The f_c's were logarithmically spaced because neural temporal-frequency tunings tend to be approximately logarithmically scaled [42–43]. The accompanying *n* factors (roughly the number of cycles per wavelet, $n = 2\pi f \cdot SD$, where *SD* is the wavelet standard deviation) were also logarithmically spaced between 3 and 16, yielding temporal resolutions ranging from *SD* = 159 ms (at 3 Hz) to *SD* = 42 ms (at 60 Hz) and spectral resolutions of *FWHM* (full width at half maximum) = 2.36 Hz (at 3 Hz) to *FWHM* = 8.83 Hz (at 60 Hz). These values struck a good balance for the time-frequency trade-off, and are typically reported in the literature [32]. The spectral-power values were then averaged within the most commonly considered frequency bands, θ (4–7 Hz), α (8–12 Hz), β (13–30 Hz), and γ (31–55 Hz). For some analyses, we also subdivided the β band into lower, β_1 (13–20 Hz), and higher, β_2 (21–30 Hz), portions.

Results

Determining spectral-power thresholds for optimal detection of isolated spectral-power activations and suppressions.

We examined the spatiotemporal dynamics of especially high spectral power, which we refer to as *activation*, and especially low spectral power, which we refer to as *suppression* (see Introduction). We defined activation as the top-i^{th}-percentile spectral power and suppression as the bottom-j^{th}-percentile spectral power. As the number of concurrently activated or suppressed

sites dynamically increases and decreases, that is, as the spatial scale of spectral-power activations and suppressions dynamically expands and contracts, focal activations and suppressions occurring exclusively at only one site are special in that they indicate relatively independent control of activation and suppression. Thus, as a first step, we calibrated activation and suppression thresholds so that instances of focal activation and suppression were detected with maximal sensitivity. Specifically, we determined the percentile thresholds that maximized the prevalence of focal activations and suppressions relative to chance levels.

For a broad range of thresholds, the instances of focal activations (the upper row in Figure 1) and focal suppressions (the lower row in Figure 1) were elevated relative to the corresponding Binomial probabilities given by $60 \cdot p(1-p)^{60-1}$, where p is the percentile threshold and 60 is the number of sites. Notably, the 8th-percentile threshold clearly maximized the instances of both focal activations and suppressions for all frequency bands and for all conditions (Figure 1). We thus defined activation as yielding the top-8th-percentile spectral power and suppression as yielding the bottom-8th-percentile spectral power (per participant per site per condition). As expected, all phase-scrambled controls conformed to the Binomial probabilities (not shown, but would yield straight horizontal lines at y = 0 in Figure 1).

Fig 1. Proportions of focal activations (top-percentile spectral power occurring exclusively at only one site) and focal suppressions (bottom-percentile spectral power occurring exclusively at only one site) as a function of percentile threshold. The proportions of focal activations (top row) and focal suppressions (bottom row) are plotted relative to the corresponding chance levels (binomial). The cooler and warmer colors indicate the lower and higher frequency bands, θ (4-7 Hz), α (8-12 Hz), β (13-30 Hz) and γ (31-55 Hz). The black lines with circular symbols show averages across the frequency bands. The columns correspond to the five behavioral conditions. For all frequency bands and for all conditions, the instances of focal activations and focal suppressions were maximized for the 8th-percentile threshold. We thus defined activation as yielding the top 8% spectral power and suppression as yielding the bottom 8% spectral power.

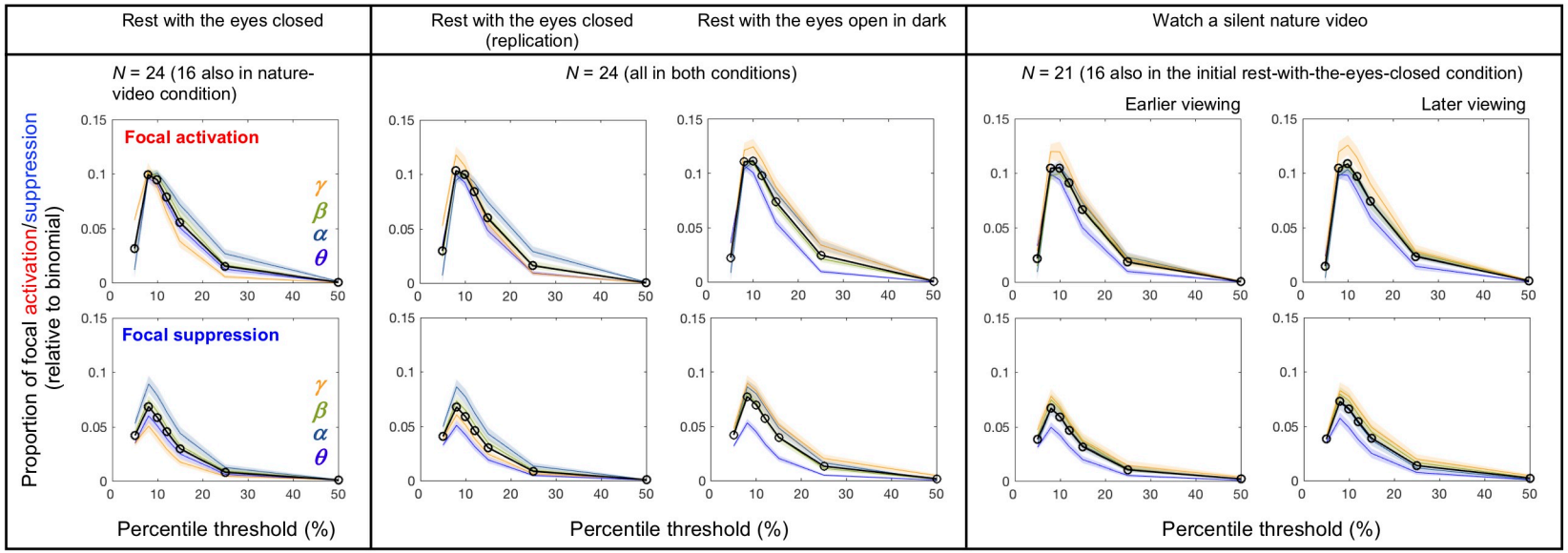
Rest with the eyes closed
Rest with the eyes closed (replication)
Rest with the eyes open in dark
Watch a silent nature video
N = 24 (16 also in nature-video condition)
N = 24 (all in both conditions)
N = 21 (16 also in the initial rest-with-the-eyes-closed condition)
Earlier viewing
Later viewing
Proportion of focal activation/suppression (relative to binomial)
Focal activation
Focal suppression
γ
β
α
θ
Percentile threshold (%)

The dynamics of the spatial scale of spectral-power activations and suppressions.

To examine the dynamics of the spatial scale of activations and suppressions, we examined the time series of the number of activated or suppressed sites, n_{sites}. Increases (or decreases) in n_{sites} indicate expansions (or contractions) in the spatial scale of activations and suppressions. An example time series of n_{sites} (from 50 sec to 100 sec) for activation and suppression for α power for one participant in the rest-with-eyes-closed condition are shown in Figure 2A–2D. The instances of small-scale (involving 1–4 sites) and large-scale (involving 10+ sites) activations and suppressions are highlighted (in red for activations and blue for suppressions). We will discuss later how these small- and large-scale activations and suppressions consistently clustered in specific regions. Even from this illustrative example it is clear that the typical durations of large-scale activations (the red highlighted portions above $n_{\text{sites}} = 10$) were substantially longer for the actual data (Figure 2A) than for the phase-scrambled control (Figure 2B). Though less apparent, one can also see that the typical durations of small-scale activations (the red highlighted portions below $n_{\text{sites}} = 4$) were longer for the actual data (Figure 2A) than for the phase-scrambled control (Figure 2B). These observations also apply to suppression. The typical durations of large-scale suppressions (the blue highlighted sections above $n_{\text{sites}} = 10$) were substantially longer for the actual data (Figure 2C) than for the phase-scrambled control (Figure 2D), and the typical durations of small-scale suppressions (the blue highlighted portions below $n_{\text{sites}} = 4$) were also longer for the actual data (Figure 2C) than for the phase-scrambled control (Figure 2D), albeit less apparent.

Average durations of small-scale ($n_{\text{sites}} \leq 4$, involving 1–4 sites), large-scale ($n_{\text{sites}} \geq 10$, involving 10+ sites), and intermediate-scale ($5 \leq n_{\text{sites}} \leq 9$, involving 5–9 sites) activations and suppressions as well as the probability distributions of n_{sites} for the rest-with-eyes-closed condition are summarized for the four frequency bands (θ, α, β, and γ) in Figure 2E–2L. For all frequency bands, the probabilities of $n_{\text{sites}} \leq 2$ and $n_{\text{sites}} \geq 10$ were elevated for both activations (Figure 2E) and suppressions (Figure 2I) relative to the binomial predictions (the black dotted curves in Figure 2E and 2I: $P_{Binom}(n_{sites}) = \frac{N!}{(N-n_{sites})!n_{sites}!} p^{n_{sites}}(1-p)^{N-n_{sites}}$, where $N = 60$ is the total number of sites, $p = 0.08$ is the threshold percentile, and n_{sites} is the number of concurrently activated or suppressed sites by chance (the data for the phase-scrambled controls conformed to the Binomial predictions [not shown]). These results suggest that focal ($n_{\text{sites}} \leq 2$) and large-scale ($n_{\text{sites}} \geq 10$) activations and suppressions are actively maintained.

Consistent with our observation above (Figure 2A–2D), the average durations of small-scale ($n_{\text{sites}} \leq 4$) activations (Figure 2F), small-scale suppressions (Figure 2J), large-scale ($n_{\text{sites}} \geq 10$)

activations (Figure 2H), and large-scale suppressions (Figure 2L) were all prolonged relative to the phase-scrambled controls (three independently phase-scrambled controls were averaged to estimate the stochastic behavior for greater reliability) for all frequency bands and for all participants (faint lines). In contrast, the average durations of intermediate-scale ($5 \leq n_{\text{sites}} \leq 9$) activations (Figure 2G) and suppressions (Figure 2K) were equivalent to the phase-scrambled controls. The average-duration results should be interpreted with the caveat that they depend on the temporal probability of event occurrences in that higher-probability events tend to have longer average durations even for stochastic variations. Nevertheless, the average duration results provide unique information in that a higher temporal probability of activations, for example, could result from either a larger number of shorter activation periods or a smaller number of longer activation periods. One can also see that the average durations were generally shorter for higher-frequency bands for both the actual data and phase-scrambled controls. This reflects the fact that the temporal resolutions of Morlet wavelets were set to be greater for higher center frequencies to achieve a reasonable time-frequency trade-off (see Methods). Nevertheless, the approximately parallel lines shown in Figure 2F–2H and 2J–2L indicate that the average durations of small-scale and large-scale activations and suppressions were prolonged by similar factors (note the logarithmic scale) regardless of frequency band. The results were the same for all of the remaining conditions: the replication of the rest-with-eyes-closed condition, the rest-with-eyes-open-in-dark condition, and the earlier and later instances of the silent-nature-video conditions (the lower four panels in Figure 2).

The results so far have shown that occurrences of focal (involving 1–2 sites) and large-scale (involving 10+ sites) activations and suppressions were increased, that the average durations of small-scale (involving 1–4 sites) and large-scale (involving 10+ sites) activations and suppressions were prolonged relative to stochastic dynamics, but that the average durations of intermediate-scale (involving 5–9 sites) activations and suppressions were equivalent to stochastic dynamics (though the average duration results need to be interpreted with a caveat; see above). These results, consistent across all frequency bands, behavioral conditions, and participants, suggest that the brain actively maintains relatively isolated small-scale networks (involving 1–4 sites) and highly cooperative large-scale networks (involving 10+ sites) of spectral-power activations and suppressions while intermediate-scale activations and suppressions tend to occur stochastically in transit.

Fig 2. Elevated instances of focal (involving 1–2 sites) and large-scale (involving 10+ sites) activations and suppressions, as well as prolonged average durations of small-scale (involving 1–4 sites) and large-scale (involving 10+ sites) activations and suppressions. Activation is defined as spectral power in the top 8% and suppression is defined as spectral power in the bottom 8% (see Figure 1). **A–D.** An example of the temporal fluctuations of the number of concurrently activated or suppressed sites for a representative participant for α power. The instances of small-scale (involving 1–4 sites) and large-scale (involving 10+ sites) activations and suppressions are highlighted. **A.** The number of activated sites as a function of time. **B.** The same as A but for the phase-scrambled control. **C.** The number of suppressed sites as a function of time. **D.** The same as C but for the phase-scrambled control. **E–L.** The probabilities and average durations of small-scale (involving 1–4 sites), intermediate-scale (involving 5–9 sites), and large-scale (involving 10+ sites) activations and suppressions for the rest-with-eyes-closed condition. The cooler and warmer colors indicate the lower and higher frequency bands, θ (4-7 Hz), α (8-12 Hz), β (13-30 Hz) and γ (31-55 Hz). The solid lines indicate the means while the faint lines show the data from individual participants. **E.** The probabilities of concurrent activations of different numbers of sites. The thick black dotted curve shows the chance (binomial) distribution. Only the actual data are shown because the phase-scrambled controls conformed to the chance distribution (not shown). Note that the instances of focal (involving 1–2 sites) and large-scale (involving 10+ sites) activations were elevated relative to chance. **F–H.** The average durations of small-scale (**F**), intermediate-scale (**G**), and large-scale (**H**) activations. Note that the average durations were prolonged for small- and large-scale (but not intermediate-scale) activations relative to the phase-scrambled controls. **I.** The probabilities of concurrent suppressions of different numbers of sites. Note that the instances of focal (involving 1–2 sites) and large-scale (involving 10+ sites) suppressions were elevated relative to chance. **J–L.** The average durations of small-scale (**J**), intermediate-scale (**K**), and large-scale (**L**) suppressions. Note that the average durations were prolonged for small- and large-scale (but not intermediate-scale) suppressions relative to the phase-scrambled controls. The remaining panels in the bottom row parallel E–L, showing the probabilities and average durations of small-, intermediate-, and large-scale activations and suppressions for the four remaining conditions. The results are nearly identical across all behavioral conditions.

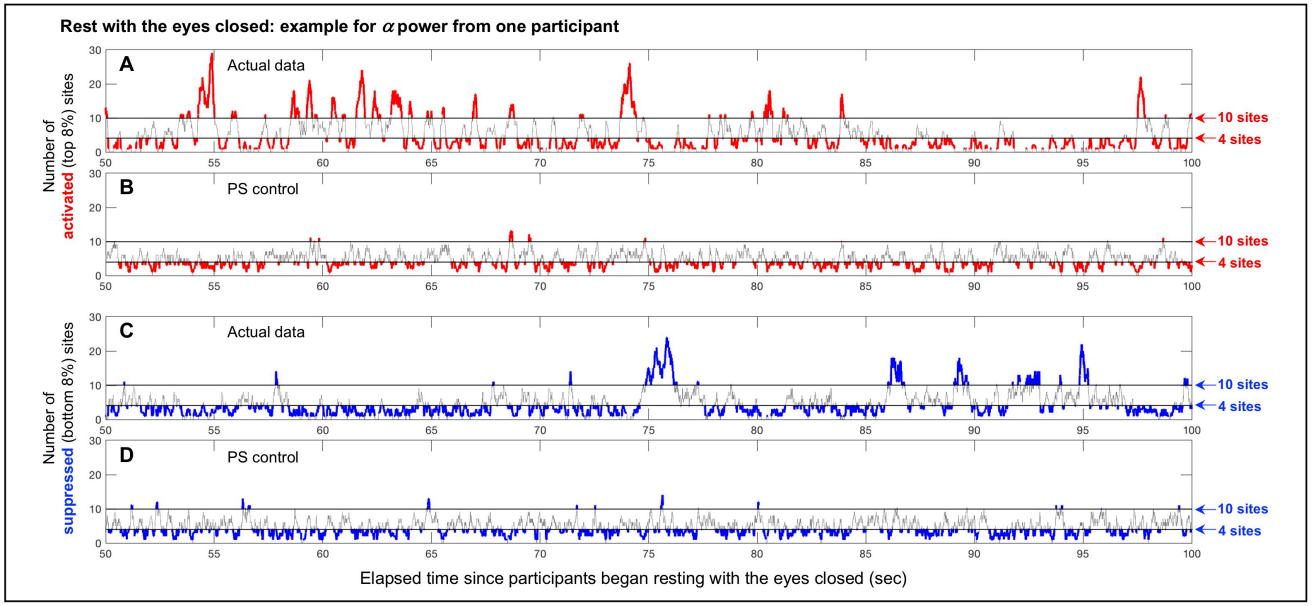
Rest with the eyes closed: example for α power from one participant
A
Actual data
B
PS control
C
Actual data
D
PS control
Number of activated (top 8%) sites
Number of suppressed (bottom 8%) sites
10 sites
4 sites
Elapsed time since participants began resting with the eyes closed (sec)

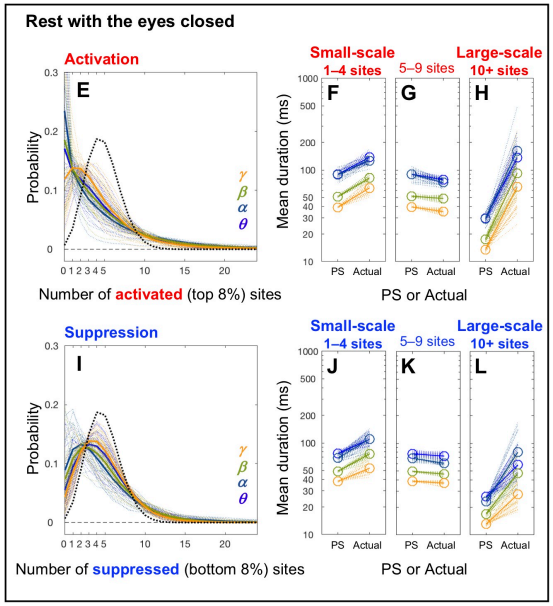
Rest with the eyes closed
Activation
Suppression
Small-scale 1–4 sites
5–9 sites
Large-scale 10+ sites
E
F
G
H
I
J
K
L
Probability
Mean duration (ms)
γ
β
α
θ
Number of activated (top 8%) sites
Number of suppressed (bottom 8%) sites
PS or Actual

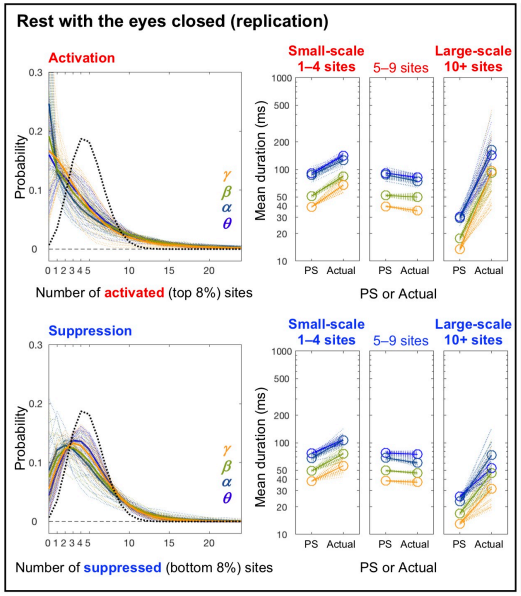
Rest with the eyes closed (replication)
Activation
Suppression
Small-scale 1–4 sites
5–9 sites
Large-scale 10+ sites
Probability
Mean duration (ms)
Number of activated (top 8%) sites
Number of suppressed (bottom 8%) sites
PS or Actual

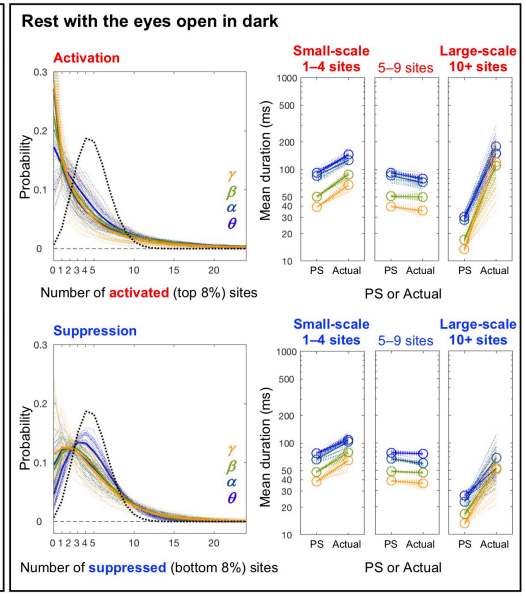
Rest with the eyes open in dark
Activation
Suppression
Small-scale 1–4 sites
5–9 sites
Large-scale 10+ sites
Probability
Mean duration (ms)
Number of activated (top 8%) sites
Number of suppressed (bottom 8%) sites
PS or Actual

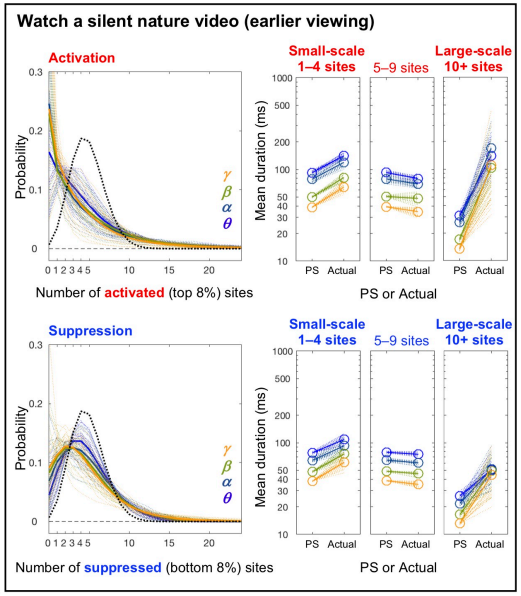
Watch a silent nature video (earlier viewing)
Activation
Suppression
Small-scale 1–4 sites
5–9 sites
Large-scale 10+ sites
Probability
Mean duration (ms)
Number of activated (top 8%) sites
Number of suppressed (bottom 8%) sites
PS or Actual

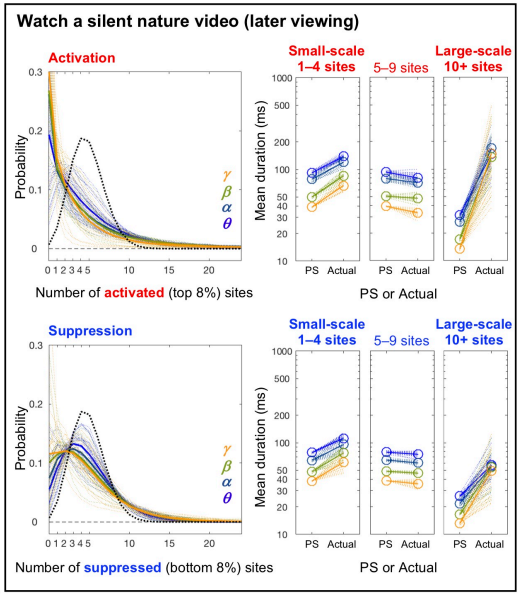
Watch a silent nature video (later viewing)
Activation
Suppression
Small-scale 1–4 sites
5–9 sites
Large-scale 10+ sites
Probability
Mean duration (ms)
Number of activated (top 8%) sites
Number of suppressed (bottom 8%) sites
PS or Actual

Spatial distributions of spectral-power activations and suppressions.

The next question we addressed was whether small-scale (involving 1–4 sites) and large-scale (involving 10+ sites) activations and suppressions clustered in specific regions. In other words, were distinct neural sub-populations preferentially involved in relatively isolated versus highly coordinated spectral-power activations and suppressions? To address this question, we examined the spatial probability distribution of activations and suppressions as a function of n_{sites} (the number of concurrently activated or suppressed sites) relative to the chance probability of 1/60 (because we used 60 sites).

The spatial probability distributions are shown for each frequency band in Figure 3 (θ), Figure 4 (α), Figure 5(β_1), Figure 6 (β_2), and Figure 7 (γ). We split β band (13–30 Hz) into the lower β_1 (13–20 Hz) and upper β_2 (21–30 Hz) sub-bands because they yielded distinct spatial probability distributions. In each figure, the rows of spatial-probability-distribution plots are organized by three behavioral conditions, resting with eyes closed (with the original and replication data combined), resting with eyes open in dark, and watching a silent nature video (with the earlier and later viewing data averaged). For each condition, the top two rows show the spatial probability distributions for activations (the upper row) and suppressions (the lower row) for increasing values of n_{sites}, measured as the proportion difference from the chance level (1/60). For instance, a value of 0.4 indicates 40% more frequent occurrences of activations or suppressions than expected by chance; a value of –0.8 indicates 80% less frequent occurrences of activations or suppressions than expected by chance. Although this provides a reasonable measure of positive and negative deviations from the chance level, the positive deviations are necessarily diluted for larger values of n_{sites} (capped at $1/n_{sites} - 1/60$) and negative deviations are floored at –1 (100% below the chance level). We thus made our inferences based on the robustness of the positive and negative deviations from the chance level computed as *t*-values (the mean probability difference from the chance level divided by the standard error with participants as the random effect). Spatial probability distributions based on *t*-values are shown in the bottom two rows for each condition (highlighted with gray-shaded rectangles and labeled A–F in Figures 3–7). The values required for Bonferroni-corrected significant (α = 0.05, 2-tailed) deviations from the chance level are indicated on the color bars. Cooler colors indicate below-chance probabilities, warmer colors indicate above-chance probabilities, and the green color indicates the chance level.

Spatial distributions of small-scale spectral-power activations and suppressions.

Small-scale (involving 1–4 sites) activations and suppressions consistently clustered in overlapping and frequency-specific regions for each condition. For the θ band, small-scale activations and suppressions clustered in the frontal and lateral-anterior regions in the eyes-closed condition (the four left columns in Figure 3A–3B), whereas they clustered in the lateral-central regions in the eyes-open conditions (the four left columns in Figure 3C–3F). For the α band, small-scale activations and suppressions clustered in the frontal and lateral-anterior regions largely across all conditions (the four left columns in Figure 4A–4F). For the β_1 band, small-scale activations and suppressions clustered in the frontal regions in the eyes-closed condition (the four left columns in Figure 5A–5B), whereas they only weakly clustered in the frontal, medial-central, and/or posterior regions in the eyes-open conditions (the four left columns in Figure 5C–5F). For the β_2 band, small-scale activations and suppressions primarily clustered in the frontal regions (potentially also in the medial-central-posterior regions) in the eyes-closed condition (the four left columns in Figure 6A–6B), whereas they clustered in the medial-central-posterior regions in the eyes-open conditions (the four left columns in Figure 6C–6F). For the γ band, small-scale activations and suppressions consistently clustered in the medial-central-posterior regions across all conditions (the four columns in Figure 7A–7F).

Overall, small-scale activations and suppressions clustered similarly across all conditions for the γ band (in the medial-central-posterior regions; Figure 7A–7F) and also for the α band (in the frontal and lateral-anterior regions; Figure 4A–4F) to some degree. In the eyes-closed condition, small-scale activations and suppressions for the θ, α, β_1, and β_2 bands consistently included the frontal sites (Figures 3–6, parts A–B). Interestingly, small-scale activations and suppressions for the β_2 band clustered similarly to the β_1 band in the eyes-closed condition (prominently in the frontal regions; compare Figure 6A–6B with 5A–5B), whereas they clustered similarly to the γ band in the eyes-open conditions (in the medial-central-posterior regions; compare Figure 6C–6F with 7C–7F). Further, for the β_2 band in the eyes-open conditions and the γ band in all conditions, focal-to-intermediate-scale activations systematically shifted from the medial-central-posterior regions to the posterior regions as the number of activated sites increased from 1 to about 9 (highlighted with red trapezoids in Figure 6C and 6E, and Figure 7A, 7C, and 7E), though suppressions did not yield this shift (Figure 6D and 6F, and Figure 7B, 7D, and 7F).

Complementary spatial distributions of small-scale and large-scale activations and suppressions.

The red-blue regions in the spatial-probability-distribution plots are roughly reversed between small-scale (involving 1–4 sites) and large-scale (involving 10+ sites) activations/suppressions (Figures 3–7, parts A–F), suggesting that large-scale (involving 10+ sites) activations and suppressions tended to cluster in the regions complementary to where small-scale activations and suppressions clustered. To statistically evaluate this spatial complementarity, we computed the vector similarity between the spatial distribution of focal activations/suppressions (involving only one activated/suppressed site) and the spatial distributions involving larger numbers of activated/suppressed sites. First, the spatial distribution for each number of activated/suppressed sites (per frequency per condition per participant) was vectorized by assigning the probability values (minus the chance level of 1/60) of the 60 sites to a 60-dimensional vector. We then computed the angle, A_n, between the vector corresponding to the focal-activation (or focal-suppression) distribution, $\vec{V}_{focal}$, and the vector corresponding to the activation (or suppression) distribution involving *n* sites, $\vec{V}_n$, that is, $A_n = acos\left(\frac{\vec{V}_{focal} \cdot \vec{V}_n}{|\vec{V}_{focal}||\vec{V}_n|}\right)$. Note that, because the spatial probability distributions (computed relative to 1/60) have zero means, A_n is equivalent to Pearson's correlation except for the $acos$ transform. For example, $A_n = 0°$ indicates that the distribution of *n*-site activations/suppressions is identical to the distribution of focal activation/suppression (up to a scalar multiplication factor), with $0° < A_n < 90°$ indicating that they are increasingly dissimilar, $A_n = 90°$ indicating that they are orthogonal (unrelated), $A_n > 90°$ indicating that they are increasingly complementary, and $A_n = 180°$ indicating a complete pattern reversal (red-blue reversal). We note that even if the dynamics of activations and suppressions were stochastic, some focal activations/suppressions would occur by chance, which could be weakly clustered in arbitrary regions; then, multi-site activations/suppressions would be statistically less likely to be detected in those regions due to our use of percentile-based thresholds to define activations and suppressions. This statistical bias may raise A_n for multi-site activations/suppressions to be slightly above 90° even when the underlying dynamics of activations and suppressions were stochastic. To discount this bias, we subtracted the A_n values computed for the phase-scrambled controls (for increased reliability, three sets of control A_n values were computed based on three independent versions of the phase-scrambled controls, then averaged) from those computed for the actual data. Regardless, the statistical bias considered here would have little impact when evaluating the spatial distributions of activations/suppressions averaged across participants such as those

shown in Figures 3–7 because any arbitrary (stochastic) clustering of focal activations/suppressions would have been inconsistent across participants so that they would have averaged out.

The A values (corrected for statistical bias) are plotted for activations and suppressions as a function of the number of concurrently activated and suppressed sites (n_{sites}) for each condition in Figures 3–7 (see the line graphs on the right side). The filled black symbols show the mean angles and the gray lines show the angles for the individual participants. The horizontal lines (red for activation and blue for suppression) just below and above 90° indicate statistically significant negative and positive deviations from 90° (Bonferroni-corrected, α = 0.05, 2-tailed, with participant as the random effect). The switch from significantly below 90° to significantly above 90° indicates the transition of multi-site-activation/suppression distributions from being similar to the focal-activation/suppression distributions to being complementary to them. For all frequency bands for all conditions, the multi-site-activation/suppression distributions for $n_{\text{sites}} \leq \sim 4$ remained similar to the focal-activation/suppression distributions (A values substantially lower than 90°), whereas the distributions for $n_{\text{sites}} \geq 10$ became complementary to the focal-activation/suppression distributions (A values substantially higher than 90°). The lines connected with open circles show the A values computed based on participant-averaged spatial-distribution vectors (rather than computing the A values per participant then averaging them across participants). The lines with open circles generally swing more widely from approaching 0° to approaching 180°, exaggerating the distribution similarity and complementarity. This means that the spatial distributions of small-scale activations/suppressions (involving 1–4 concurrently activated/suppressed sites) and the complementary spatial distributions of large-scale activations/suppressions (involving 10+ concurrently activated/suppressed sites) were consistent across participants (thus some of the measurement noise averaged out when the A values were computed based on the participant-averaged spatial distributions). In contrast, if each participant had his/her unique complementary distributions of small-scale and large-scale activations/suppressions, the open-circle lines would have been flat at y = 90°. This analysis confirms that large-scale (involving 10+ sites) spectral-power activations/suppressions clustered in regions that were complementary to where small-scale (involving 1–4 sites) spectral-power activations/suppressions clustered.

Spatial distributions of large-scale spectral-power activations and suppressions.

Where did large-scale (involving 10+ sites) activations and suppressions cluster by frequency band? For the θ band, they clustered in the posterior regions in the rest-with-eyes-

closed condition (Figure 3A–3B), whereas they clustered in the frontal and/or lateral-anterior regions in the rest-with-eyes-open-in-dark condition (Figure 3C–3D). In the silent-nature-video condition, intermediate- to large-scale activations clustered in the posterior to lateral-anterior regions (Figure 3E), whereas large-scale suppressions clustered in the posterior regions (Figure 3F).

For the α band, large-scale activations and suppressions clustered in the posterior and medial-anterior regions in the rest-with-eyes-closed condition (Figure 4A–4B). These patterns overall replicated in both eyes-open conditions except that the medial-anterior cluster was weak in the rest-with-eyes-open-in-dark condition (Figure 4C–4D) and both the posterior and medial-anterior clusters were weaker and the posterior cluster for activations was centrally shifted in the silent-nature-video condition (Figure 4E–4F).

For the β_1 band, large-scale activations clustered in the posterior-to-lateral-posterior and lateral-anterior regions (Figure 5A), whereas large-scale suppressions clustered in the posterior regions (Figure 5B) in the rest-with-the-eyes-closed condition. Large-scale activations also clustered in the posterior and lateral-anterior regions in the rest-with-the-eyes-open-in-dark condition (Figure 5C), whereas large-scale suppressions primarily clustered in the lateral-anterior regions (Figure 5D). In the silent-nature-video condition, large-scale activations clustered in the posterior and lateral-posterior regions (Figure 5E), whereas large-scale suppressions clustered in the lateral-anterior regions (Figure 5F).

For the β_2 band, large-scale activations and suppressions clustered in the lateral-posterior and lateral-anterior regions (Figure 6A–6B) in the rest-with-the-eyes-closed condition. In the two eyes-open conditions large-scale activations and suppressions both clustered in the lateral-anterior regions (Figure 6C–6F).

For the γ band, the spatial distributions of activations and suppressions in all conditions (Figure 7A–7F) were essentially the same as those for β_2 band in the two eyes-open conditions (Figure 6C–6F), clustering in the lateral-anterior regions (Figure 7A–7F).

Fig 3. Spatial-probability distributions of spectral-power activations and suppressions as a function of the number of concurrently activated/suppressed sites for the θ band (4–7 Hz). Activation and suppression are defined as spectral power in the top and bottom 8% (see Figure 1). The major row divisions correspond to the three behavioral conditions. For each condition, the spatial-probability-distribution plots are presented in four rows (row 1–row 4). Row 1 shows the spatial-probability distributions of activations for increasing numbers of concurrently activated sites. Small-scale (involving 1–4 sites) and large-scale (involving 10+ sites) activations are indicated because their average durations were prolonged (Figure 2). The above- and below-chance occurrences of activations are color-coded with warmer and cooler colors, with the green color indicating the chance level. The values indicate the proportions of deviations from the chance level (1/60); for example, +0.3 indicates 30% more frequent occurrences than expected by chance, whereas –0.6 indicates 60% less frequent occurrences than expected by chance. Row 2 presents the spatial-probability distributions of suppressions instead of activation. Rows 3 and 4 are identical to rows 1 and 2 except that they present the consistency of deviations from the chance level as *t*-values with the critical values for Bonferroni-corrected statistical significance (α = 0.05, 2-tailed) shown on the color bars. We focused on these *t*-value plots (highlighted and labeled **A**–**F**) for making inferences (see main text). In most cases, all participants yielded concurrent activations and suppressions involving up to 18 sites, but in some cases some participants yielded concurrent activations or suppressions involving fewer sites. In those cases, the spatial-probability-distribution plots are presented up to the maximum number of concurrently activated or suppressed sites to which all participants contributed. One can see that small-scale activations and suppressions (columns 1–4) occurred in specific regions while large-scale activations and suppressions (columns 10+) generally occurred in the complementary regions (**A**–**F**). This spatial complementarity between small- and large-scale activations and suppressions is quantified in the accompanying line graphs on the right, plotting the vector angles (in degrees) between the distribution of focal activations/suppressions and the distributions of multi-site activations/suppressions involving increasing numbers of sites. Values less than 90° indicate that multi-site activation/suppression distributions were spatially similar to focal activation/suppression distributions (with 0° indicating that they were identical up to a scalar factor), 90° indicates that multi-site distributions were orthogonal (unrelated) to focal distributions, and values greater than 90° indicate that multi-site distributions were increasingly spatially complementary to focal distributions (with 180° indicating a complete red-blue reversal). The thick lines with filled symbols indicate the mean angles and the gray lines show the data from individual participants. Bonferroni-corrected statistical significance (α = 0.05, 2-tailied) for the negative and positive deviations from 90° are indicated with the horizontal lines just below and above the dashed line indicating 90°. The lines with open symbols show the vector angles computed from the participant-averaged spatial-probability distributions.

Fig 4. Spatial-probability distributions of spectral-power activations and suppressions as a function of the number of activated/suppressed sites for the α band (8-12 Hz). The formatting is the same as in Figure 3.

Fig 5. Spatial-probability distributions of spectral-power activations and suppressions as a function of the number of activated/suppressed sites for the β_1 band (13-20 Hz). The formatting is the same as in Figures 3 and 4.

Fig 6. Spatial-probability distributions of spectral-power activations and suppressions as a function of the number of activated/suppressed sites for the β_2 band (21-30 Hz). The formatting is the same as in Figures 3–5.

Fig 7. Spatial-probability distributions of spectral-power activations and suppressions as a function of the number of activated/suppressed sites for the γ band (31-55 Hz). The formatting is the same as in Figures 3–6.

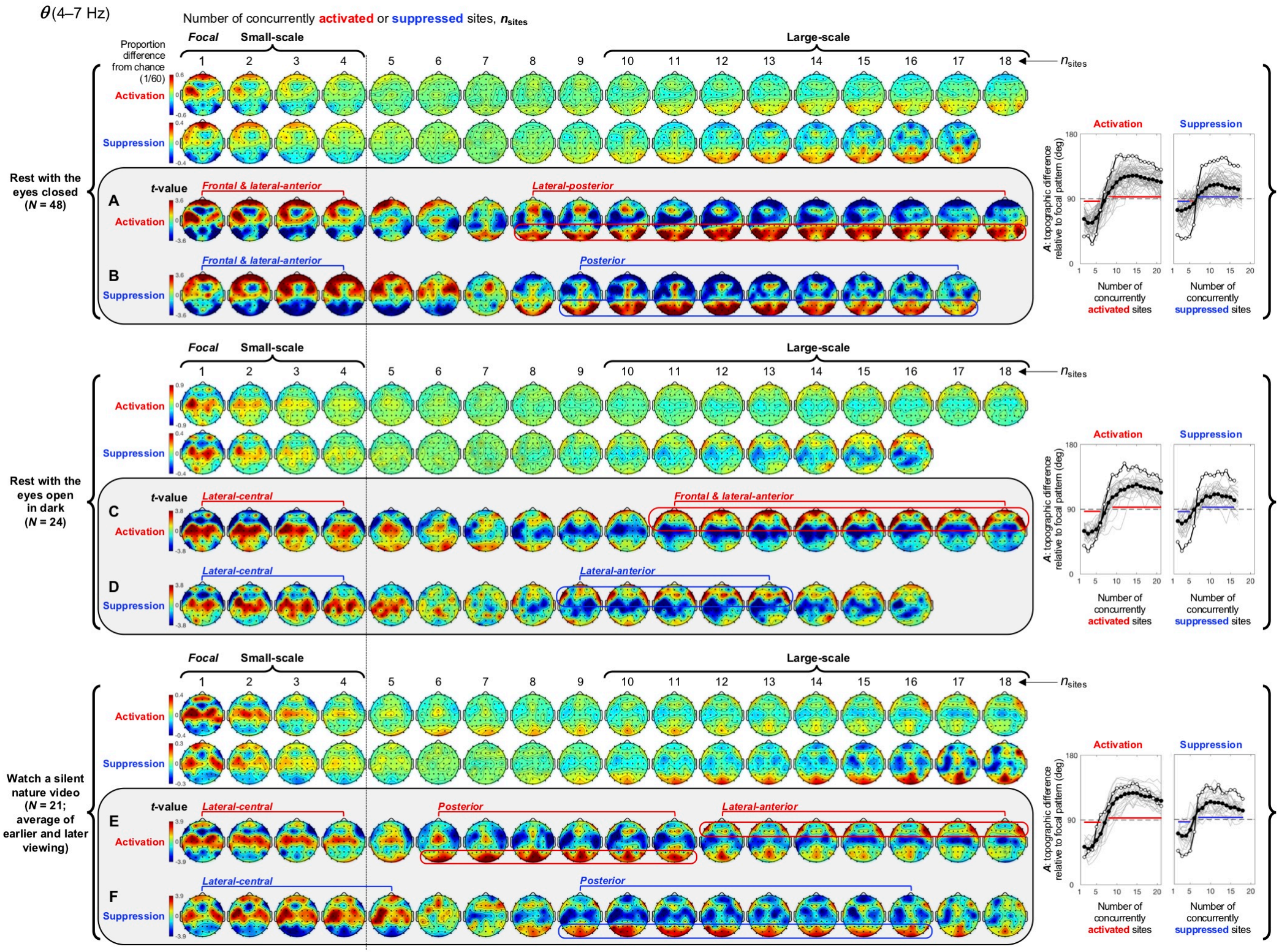
θ (4–7 Hz)
Number of concurrently activated or suppressed sites, n_{sites}
Proportion difference from chance (1/60)
Focal
Small-scale
Large-scale
n_{sites}
Activation
Suppression
t-value
A
B
C
D
E
F
Frontal & lateral-anterior
Lateral-posterior
Posterior
Lateral-central
Lateral-anterior
A: topographic difference relative to focal pattern (deg)
Number of concurrently activated sites
Number of concurrently suppressed sites
Rest with the eyes closed (N = 48)
Rest with the eyes open in dark (N = 24)
Watch a silent nature video (N = 21; average of earlier and later viewing)

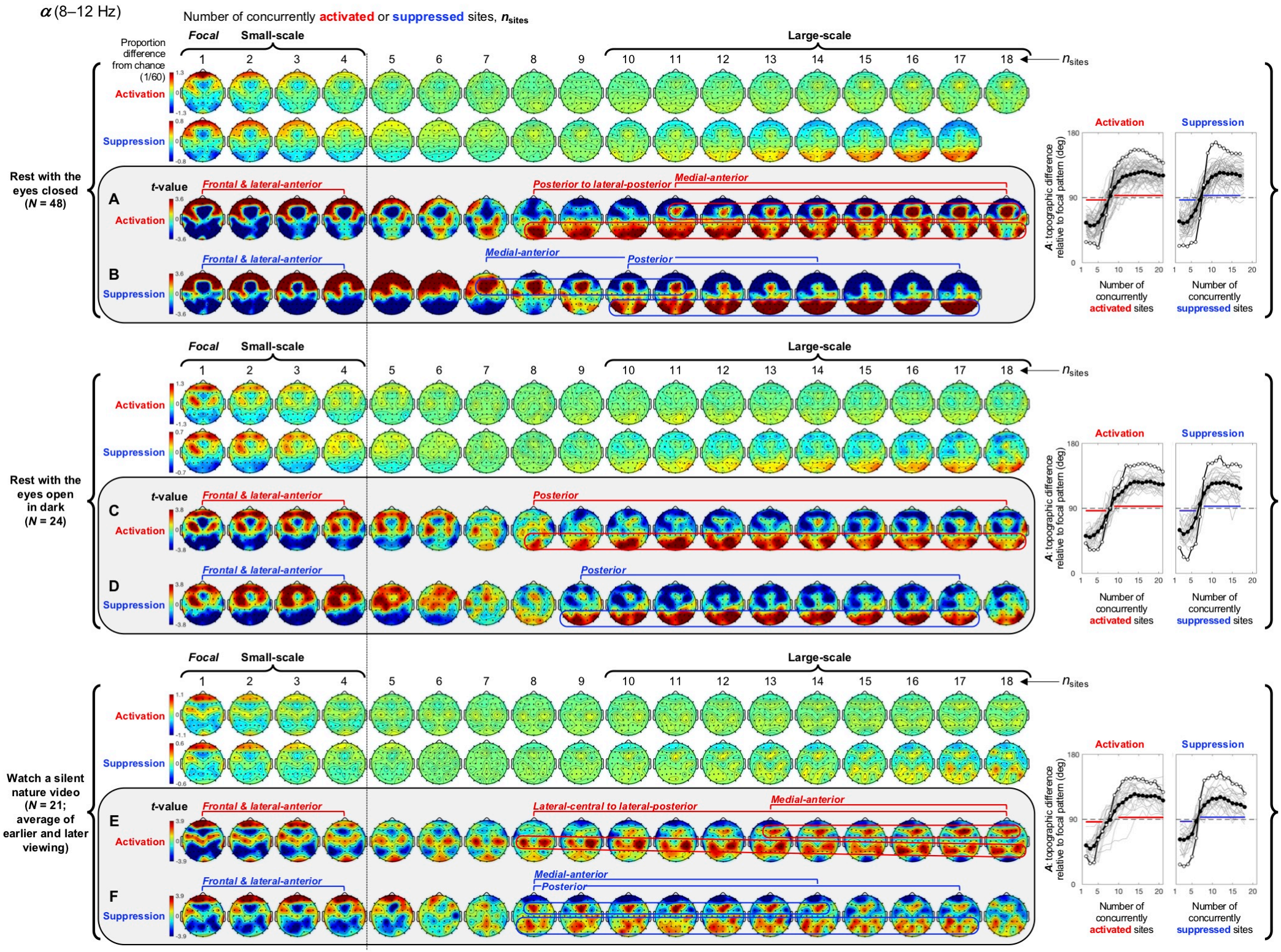
α (8–12 Hz)
Number of concurrently activated or suppressed sites, n_{sites}
Proportion difference from chance (1/60)
Focal
Small-scale
Large-scale
n_{sites}
Activation
Suppression
Rest with the eyes closed (N = 48)
t-value
A
B
Frontal & lateral-anterior
Posterior to lateral-posterior
Medial-anterior
Posterior
Rest with the eyes open in dark (N = 24)
C
D
Watch a silent nature video (N = 21; average of earlier and later viewing)
E
F
Lateral-central to lateral-posterior
A: topographic difference relative to focal pattern (deg)
Number of concurrently activated sites
Number of concurrently suppressed sites

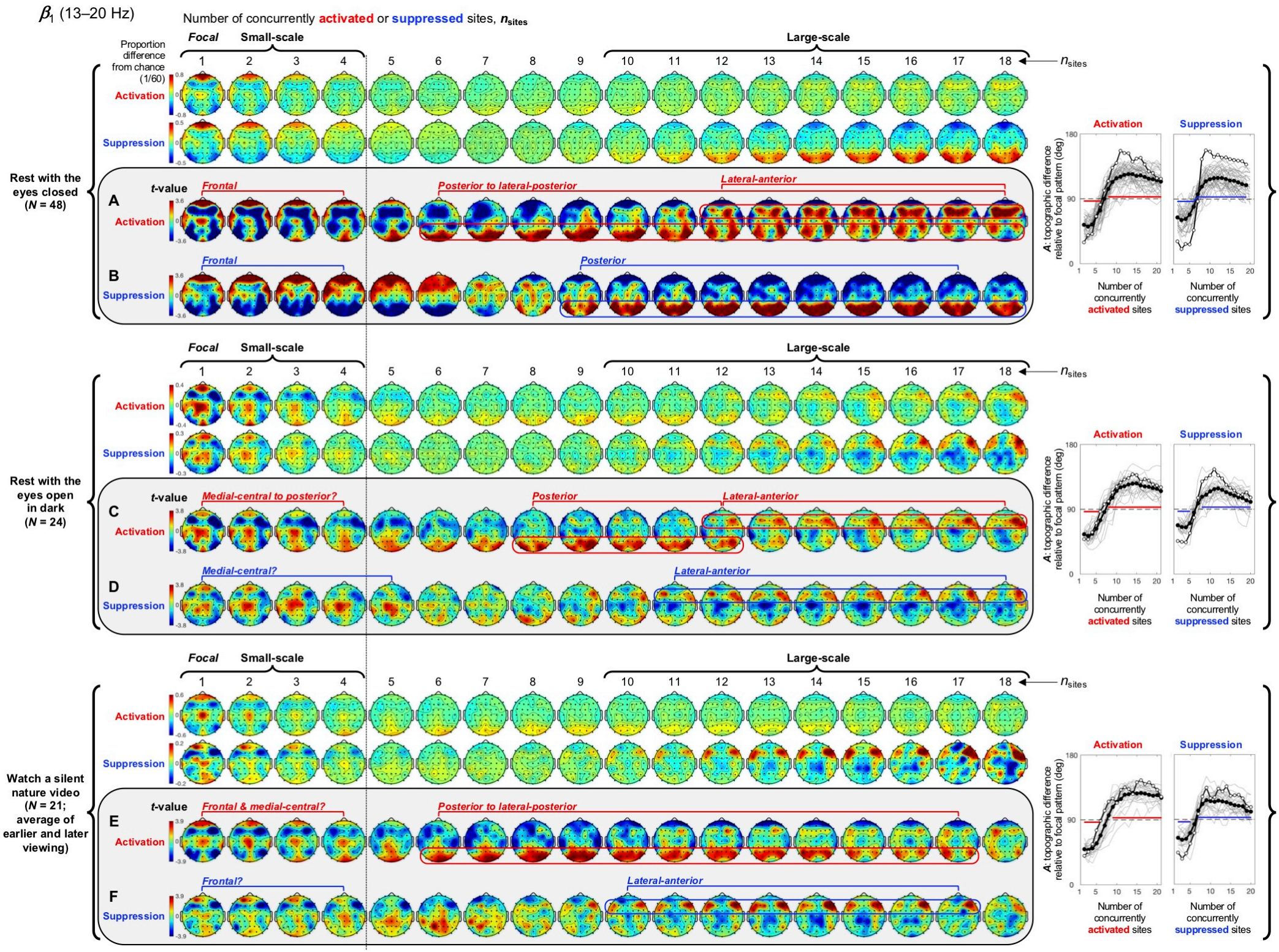
β_1 (13–20 Hz)
Number of concurrently activated or suppressed sites, n_{sites}
Proportion difference from chance (1/60)
Focal
Small-scale
Large-scale
n_{sites}
Activation
Suppression
Rest with the eyes closed (N = 48)
t-value
A
B
Frontal
Posterior to lateral-posterior
Lateral-anterior
Posterior
Rest with the eyes open in dark (N = 24)
C
D
Medial-central to posterior?
Medial-central?
Watch a silent nature video (N = 21; average of earlier and later viewing)
E
F
Frontal & medial-central?
Frontal?
A: topographic difference relative to focal pattern (deg)
Number of concurrently activated sites
Number of concurrently suppressed sites

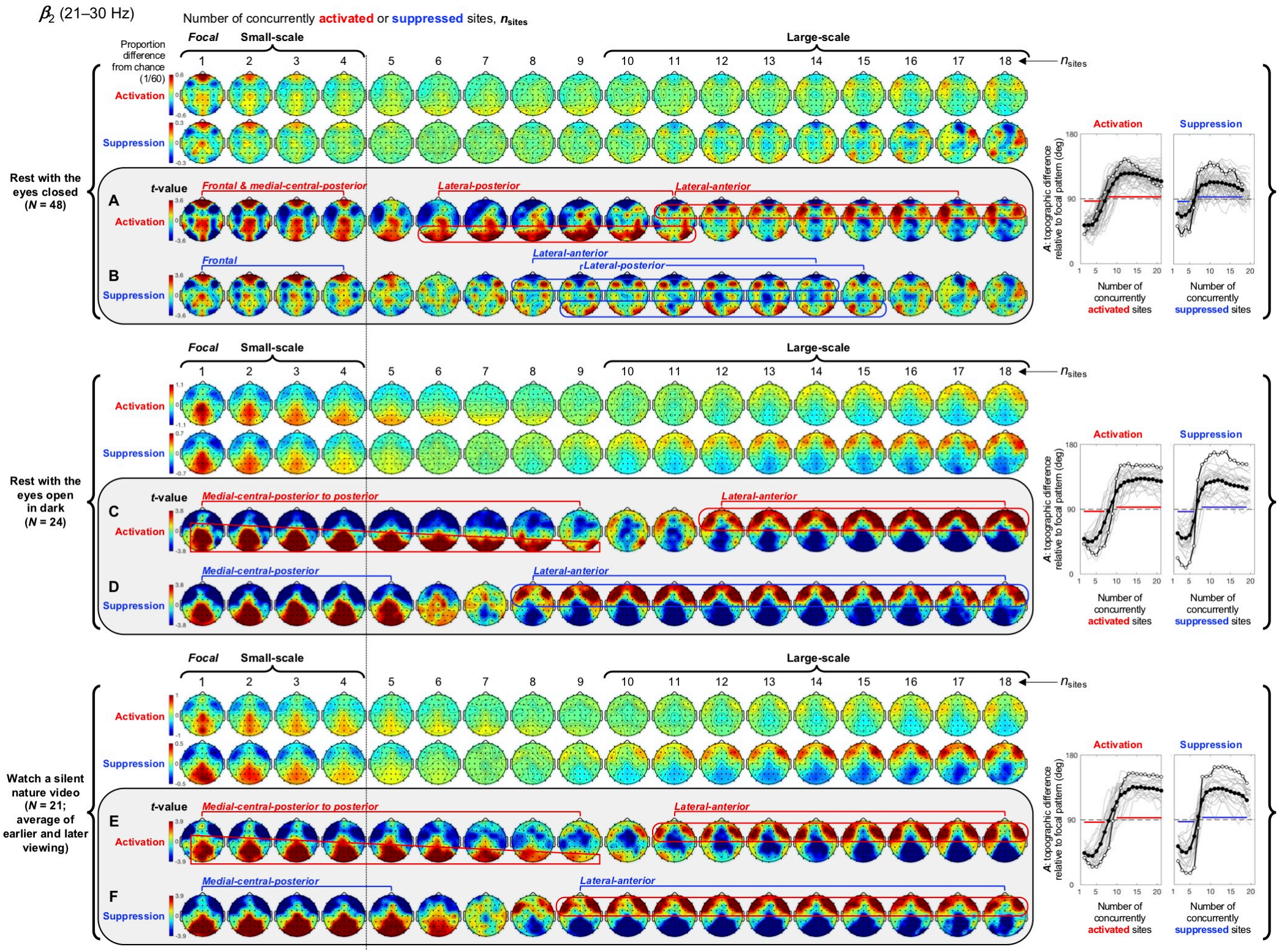
β_2 (21–30 Hz)
Number of concurrently activated or suppressed sites, n_{sites}
Proportion difference from chance (1/60)
Focal
Small-scale
Large-scale
n_{sites}
Activation
Suppression
Rest with the eyes closed (N = 48)
t-value
A
B
Frontal & medial-central-posterior
Lateral-posterior
Lateral-anterior
Frontal
Rest with the eyes open in dark (N = 24)
C
D
Medial-central-posterior to posterior
Medial-central-posterior
Watch a silent nature video (N = 21; average of earlier and later viewing)
E
F
A: topographic difference relative to focal pattern (deg)
Number of concurrently activated sites
Number of concurrently suppressed sites

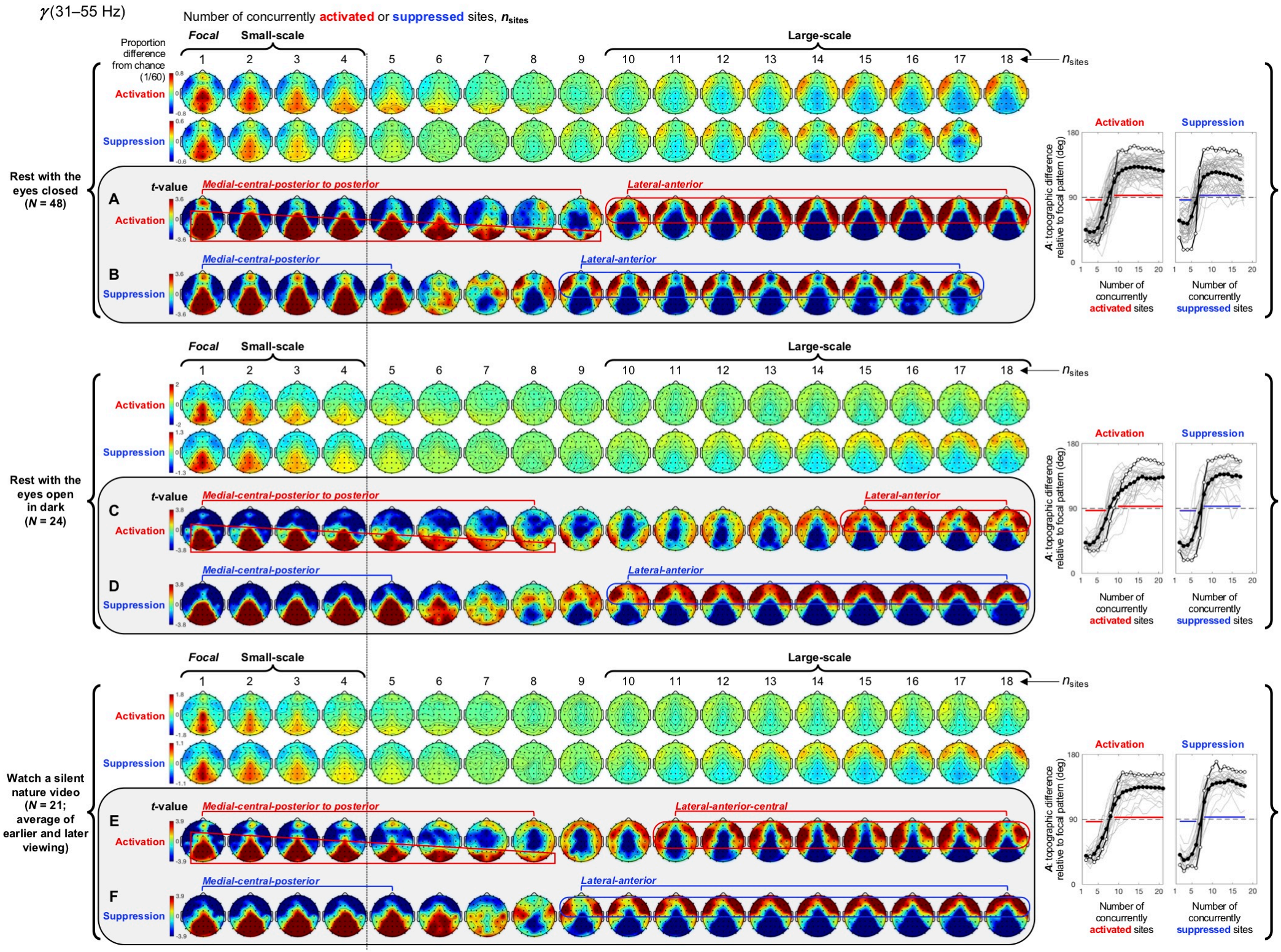
γ(31–55 Hz)
Number of concurrently activated or suppressed sites, n_{sites}
Proportion difference from chance (1/60)
Focal
Small-scale
Large-scale
n_{sites}
Activation
Suppression
Rest with the eyes closed (N = 48)
Rest with the eyes open in dark (N = 24)
Watch a silent nature video (N = 21; average of earlier and later viewing)
t-value
A
B
C
D
E
F
Medial-central-posterior to posterior
Lateral-anterior
Medial-central-posterior
Lateral-anterior-central
A: topographic difference relative to focal pattern (deg)
Number of concurrently activated sites
Number of concurrently suppressed sites

Contextual effects on the spatial distributions of spectral-power activations and suppressions.

How did the clustering of activations and suppressions depend on context? The spatial scale of activations and suppressions (as indexed by the number of concurrently activated/suppressed sites, n_{sites}) remained small or large sometimes, but rapidly expanded from small to large or contracted from large to small other times (e.g., Figure 2A–2D). Are the distributions of activations and suppressions influenced by these temporal contexts?

Activations and suppressions both yielded the characteristic average distributions (including all contexts) shown in Figures 3–7 when they fluctuated within the small-scale (1–4 sites) range or within the large-scale (10+ sites) range (the thick straight arrows in Figures 8–12 [for the θ, α, β_1, β_2, and γ bands], part A [for activations] and part E [for suppressions] for each condition). In some cases, activations also yielded consistent distributions when they fluctuated within the intermediate-scale (5–9 sites) range (the thin straight arrows in Figures 8–12, part A for each condition), though suppressions rarely yielded consistent distributions while fluctuating within the intermediate-scale range (the thin straight arrows in Figures 8–12, part E for each condition). When activations and suppressions fluctuated between the small-scale (1–4 sites) and intermediate-scale (5–9 sites) ranges (e.g., monotonically increasing from 2 sites to 8 sites, monotonically decreasing from 7 sites to 1 site, etc.), they tended to yield characteristic small-scale distributions (the curved arrows in Figures 8–12, part B [for activations] and part F [for suppressions] for each condition). In all these cases where activations and suppressions fluctuated within a specific spatial-scale range (small, intermediate, or large) or fluctuated between the small- and intermediate-scale ranges, we did not observe any directional asymmetry; that is, the distributions of activations and suppressions were virtually identical in the contexts of their spatial expansions and contractions (data not shown).

For extensive expansions and contractions of activations and suppressions, we observed some directional dependence so that the expansions from the small-scale (1–4 sites) range to the large-scale (10+ sites) range (e.g., monotonically increasing from 3 sites to 15 sites) and the contractions from the large-scale (10+ sites) range to the small-scale (1–4 sites) range (e.g., monotonically decreasing from 12 sites to 2 sites) are shown separately (Figures 8-12 part C [for expansions] and part D [for contractions]). Nevertheless, general characteristics are observed for both expansions and contractions. During the extensive spatial expansions and contractions of activations (the unidirectional curved arrows in Figures 8–12, part C [for expansions] and part D [for contractions] for each condition), some consistent distributions were observed in the intermediate- and large-scale ranges including some of the characteristic large-

scale distributions we saw in Figures 3–7, but no consistent distributions were observed in the small-scale range. During the extensive spatial expansions and contractions of suppressions (the unidirectional curved arrows in Figures 8–12, parts G [for expansions] and H [for contractions] for each condition), no consistent distributions were observed in any spatial scale.

Overall, the context analysis yielded two notable results. First, the characteristic distributions of activations and suppressions shown in Figures 3–7 were especially consistent while the spatial scale of activations and suppressions remained within the small-scale or large-scale range, with the intermediate-scale distributions largely being transitional. Second, some of the characteristic large-scale, but not small-scale, distributions of activations shown in Figures 3–7 occurred during extensive expansions and contractions of activations, whereas no consistent distributions of suppressions occurred in any spatial scale during extensive expansions or contractions of suppressions.

Fig 8. Context effects on the spatial distributions of spectral-power activations and suppressions for the θ band (4–7 Hz). As in Figures 3–7, activation and suppression are defined as spectral power in the top and bottom 8%, and the major row divisions correspond to the three behavioral conditions. **A and E per condition.** Spatial distributions of activations (**A**) and suppressions (**E**) when the number of concurrently activated or suppressed sites fluctuated within the small-scale (1–4 sites), intermediate-scale (5–9 sites), or large-scale (10+ sites) range (highlighted). **B and F per condition.** Spatial distributions of activations (**B**) and suppressions (**F**) when the number of concurrently activated or suppressed sites fluctuated between the small-scale (1–4 sites) and intermediate-scale (5–9 sites) ranges. **C and G per condition.** Spatial distributions of activations (**C**) and suppressions (**G**) when the number of concurrently activated or suppressed sites extensively expanded from the small-scale (1–4 sites) to large-scale (10+ sites) range. **D and H per condition.** Spatial distributions of activations (**D**) and suppressions (**H**) when the number of concurrently activated or suppressed sites extensively contracted from the large-scale (10+ sites) to small-scale (1–4 sites) range. All spatial distributions are shown in *t*-values as in Figures 3–7, parts A–E. Spatial-distribution plots are shown only for the cases where all participants contributed to the corresponding data.

Fig 9. Context effects on the spatial distributions of spectral-power activations and suppressions for the α band (8-12 Hz). The formatting is the same as in Figure 8. No plots are shown in **G** for the rest-with-the-eyes-closed condition because none of the relevant expansions of suppressions had data from all participants.

Fig 10. Context effects on the spatial distributions of spectral-power activations and suppressions for the β_1 band (13-20 Hz). The formatting is the same as in Figures 8 and 9.

Fig 11. Context effects on the spatial distributions of spectral-power activations and suppressions for the β_2 band (21-30 Hz). The formatting is the same as in Figures 8–10.

Fig 12. Context effects on the spatial distributions of spectral-power activations and suppressions for the γ band (31-55 Hz). The formatting is the same as in Figures 8–11.

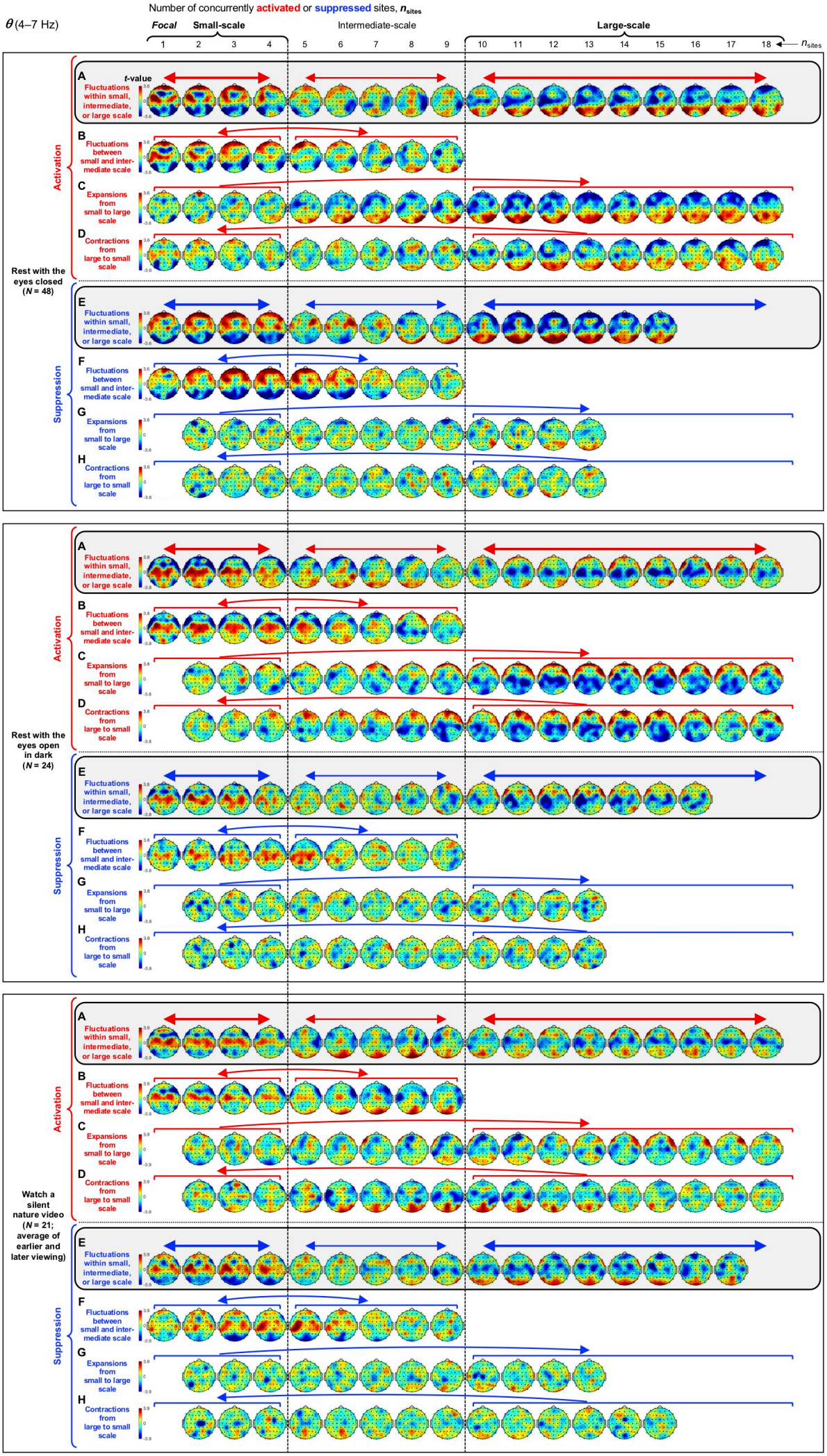
θ (4–7 Hz)
Number of concurrently activated or suppressed sites, n_{sites}
Focal
Small-scale
Intermediate-scale
Large-scale
1 2 3 4 5 6 7 8 9 10 11 12 13 14 15 16 17 18
n_{sites}
t-value
Activation
Suppression
A Fluctuations within small, intermediate, or large scale
B Fluctuations between small and intermediate scale
C Expansions from small to large scale
D Contractions from large to small scale
E Fluctuations within small, intermediate, or large scale
F Fluctuations between small and intermediate scale
G Expansions from small to large scale
H Contractions from large to small scale
Rest with the eyes closed (N = 48)
Rest with the eyes open in dark (N = 24)
Watch a silent nature video (N = 21; average of earlier and later viewing)

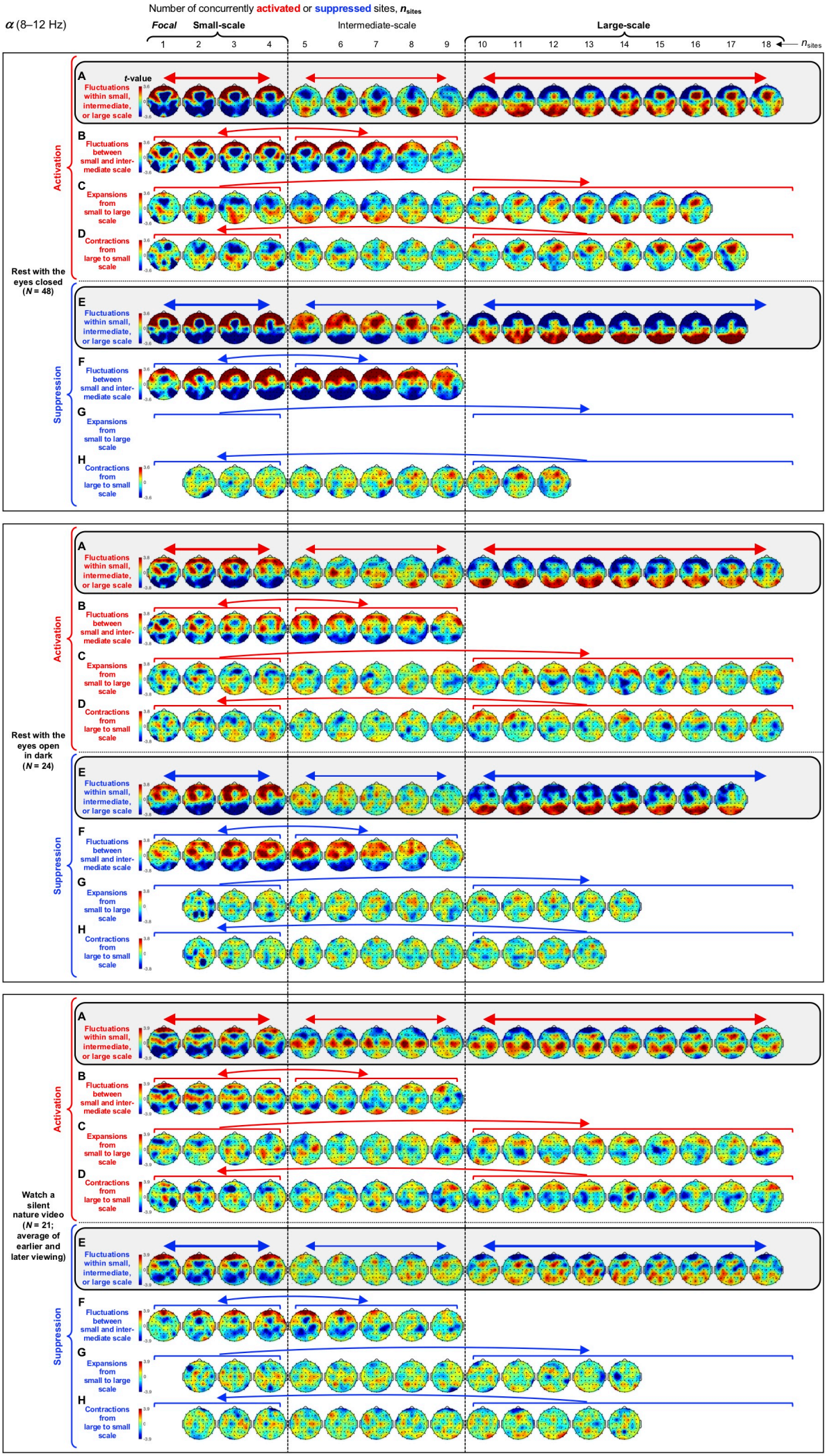
α (8–12 Hz)
Number of concurrently activated or suppressed sites, n_{sites}
Focal
Small-scale
Intermediate-scale
Large-scale
1 2 3 4 5 6 7 8 9 10 11 12 13 14 15 16 17 18
n_{sites}
t-value
Activation
Suppression
A Fluctuations within small, intermediate, or large scale
B Fluctuations between small and intermediate scale
C Expansions from small to large scale
D Contractions from large to small scale
E Fluctuations within small, intermediate, or large scale
F Fluctuations between small and intermediate scale
G Expansions from small to large scale
H Contractions from large to small scale
Rest with the eyes closed (N = 48)
Rest with the eyes open in dark (N = 24)
Watch a silent nature video (N = 21; average of earlier and later viewing)

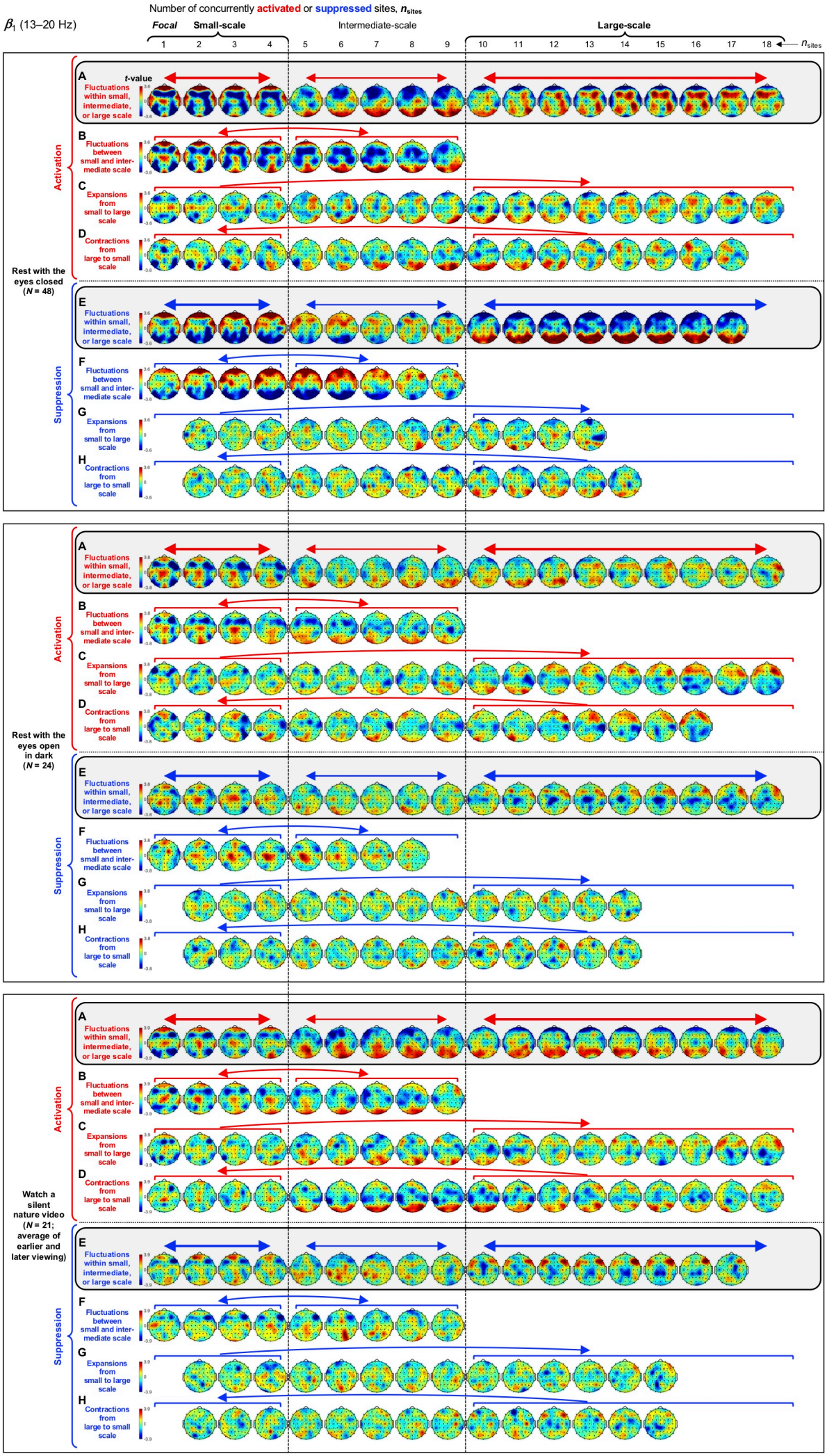
β_1 (13–20 Hz)
Number of concurrently activated or suppressed sites, n_{sites}
Focal
Small-scale
Intermediate-scale
Large-scale
1 2 3 4 5 6 7 8 9 10 11 12 13 14 15 16 17 18
n_{sites}
t-value
Activation
Suppression
A Fluctuations within small, intermediate, or large scale
B Fluctuations between small and intermediate scale
C Expansions from small to large scale
D Contractions from large to small scale
E Fluctuations within small, intermediate, or large scale
F Fluctuations between small and intermediate scale
G Expansions from small to large scale
H Contractions from large to small scale
Rest with the eyes closed (N = 48)
Rest with the eyes open in dark (N = 24)
Watch a silent nature video (N = 21; average of earlier and later viewing)

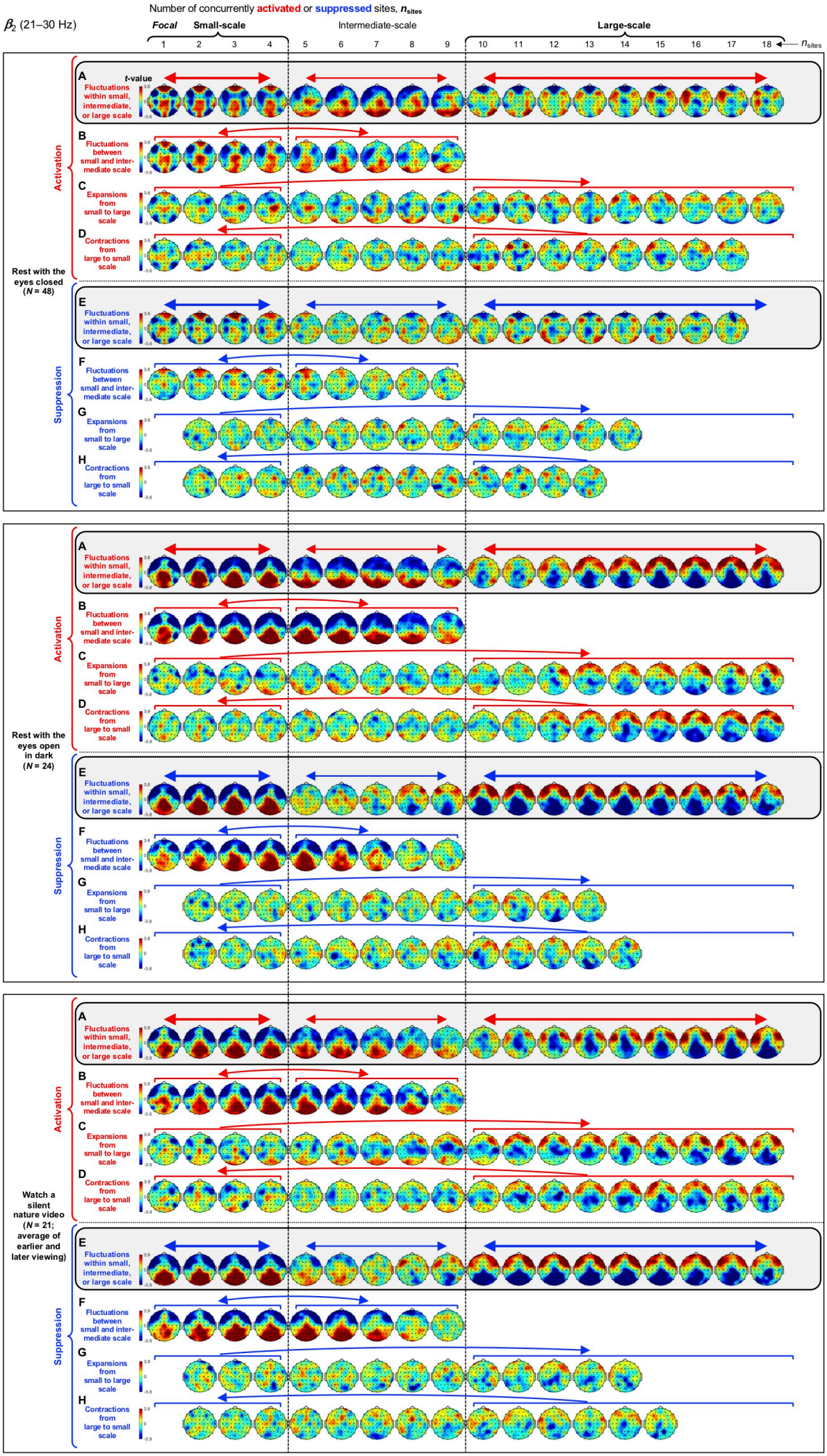
β_2 (21–30 Hz)
Number of concurrently activated or suppressed sites, n_{sites}
Focal
Small-scale
Intermediate-scale
Large-scale
1 2 3 4 5 6 7 8 9 10 11 12 13 14 15 16 17 18
n_{sites}
t-value
Activation
Suppression
A Fluctuations within small, intermediate, or large scale
B Fluctuations between small and intermediate scale
C Expansions from small to large scale
D Contractions from large to small scale
E Fluctuations within small, intermediate, or large scale
F Fluctuations between small and intermediate scale
G Expansions from small to large scale
H Contractions from large to small scale
Rest with the eyes closed (N = 48)
Rest with the eyes open in dark (N = 24)
Watch a silent nature video (N = 21; average of earlier and later viewing)

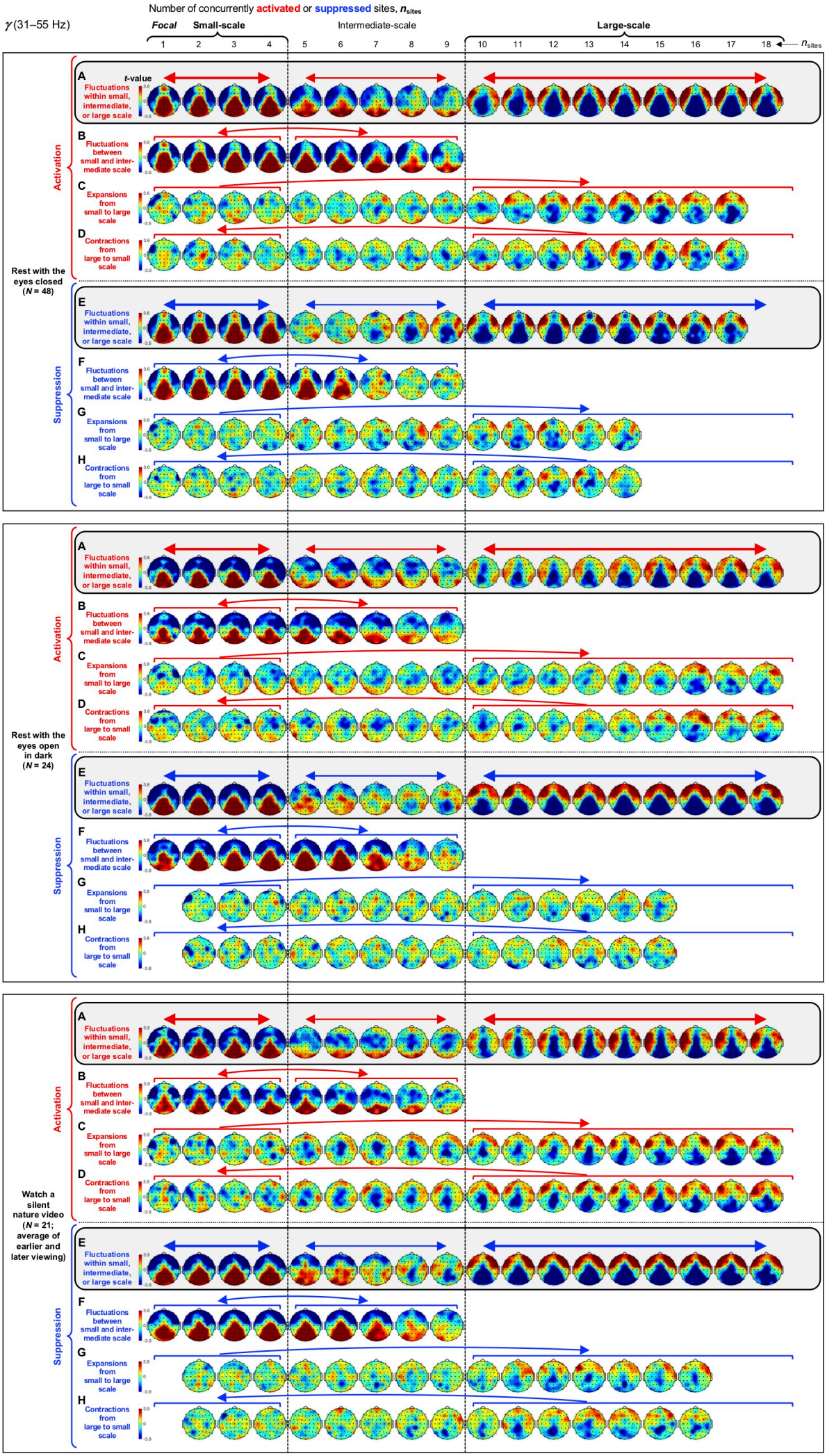
γ (31–55 Hz)
Number of concurrently activated or suppressed sites, n_{sites}
Focal
Small-scale
Intermediate-scale
Large-scale
1 2 3 4 5 6 7 8 9 10 11 12 13 14 15 16 17 18
n_{sites}
t-value
Activation
Suppression
A Fluctuations within small, intermediate, or large scale
B Fluctuations between small and intermediate scale
C Expansions from small to large scale
D Contractions from large to small scale
E Fluctuations within small, intermediate, or large scale
F Fluctuations between small and intermediate scale
G Expansions from small to large scale
H Contractions from large to small scale
Rest with the eyes closed (N = 48)
Rest with the eyes open in dark (N = 24)
Watch a silent nature video (N = 21; average of earlier and later viewing)

Temporal correlations of the number of activated/suppressed sites between frequency bands.

We have seen that the spatial scale of spectral-power activations and suppressions dynamically vary between characteristic small-scale and large-scale patterns that are frequency specific (Figure 2A-D; Figures 3–7). Are the engagements of small- and large-scale networks independent or coordinated across frequency bands? To address this question, we computed the temporal correlation of n_{site} (the number of concurrently activated or suppressed sites) between each pair of frequency bands, using Spearman's r, r_{sp} (which is outlier resistant). To alleviate any effect of spectral leakage (due to the wavelet spectral-tuning widths; see Methods), we computed the baseline-corrected $\underline{r}_{sp}$ by subtracting from r_{sp} the baseline r_{sp} computed with the phase-scrambled data (an average of three baseline r_{sp} values computed based on three independent versions of phase-scrambled data).

Figure 13 presents the correlation matrices (symmetric about the diagonal) for activations (Figure 13A–13E) and suppressions (Figure 13K–13O) for each of the five behavioral conditions. The correlation patterns were generally similar for activations and suppressions. All average correlations were positive (lighter colors indicating stronger correlations) and statistically significant (p<0.05, two-tailed, Bonferroni corrected, based on $\underline{r}_{sp}$ computed with Fisher-Z transformed r_{sp} and baseline r_{sp} values), except for those indicated with the white "-" symbols. The temporal correlations of n_{sites} were modest (avaraging less than 0.5) and generally diminished with greater separations of frequencies (the cells further away from the diagonal are darker). The θ –β_2, θ–γ, and α–γ correlations were especially weak as evident from the dark colored cells in the upper-right and lower-left corners of all correlation matrices (Figure 13).

The correlation matrices for both activations and suppressions also characteristically differed between the eyes-closed (rest-with-eyes-closed) and eyes-open (rest-with-eyes-open-in-dark and watch-a-silent-nature-video) conditions. Each of the eyes-closed matrices (Figure 13A and 13B for activations, and 13K and 13L for suppressions) is characterized by a large central region of lighter cells indicative of elevated correlations among α, β_1, and β_2 bands (highlighted with a large dashed central square), whereas each of the eyes-open matrices (Figure 13C–13E for activations, and 13M–13O for suppressions) is characterized by a pair of square regions of lighter cells indicative of elevated correlations between α and β_1 bands and between β_2 and γ bands (highlighted with two small dashed squares). To quantitatively evaluate these two patterns, we compared the $\underline{r}_{sp}$ values (computed with Fisher-Z transformed r_{sp} and baseline r_{sp} values) among the cells labeled 1, 2, and 3. The large central-square pattern is distinguished by relatively higher $\underline{r}_{sp}$ values in cells 1 and 2 and lower $\underline{r}_{sp}$ values in cells 3. Although this pattern is

not particularly strong in the eyes-closed conditions (Figure 13F and13G for activations, and 13P and 13Q for suppressions), the average $\underline{r}_{sp}$ values were always lowest in cells 3. The reason why the $\underline{r}_{sp}$ values were not substantially lower in cells 3 is that some of the participants yielded the opposite pattern corresponding to the eyes-open conditions with high correlations in cells 3 (see the thin lines showing the data from individual participants in Figure 13). The double-small-square pattern is distinguished by higher $\underline{r}_{sp}$ values in cells 1 and 3 and lower $\underline{r}_{sp}$ values in cells 2. This V-shaped pattern was consistently observed in the eyes-open conditions (Figure 13H–13J for activations, and 13R–13T for suppressions).

Thus, we obtained some evidence for coordinated engagements of the small-scale and large-scale synchronization networks between frequency bands (as temporal correlations of n_{sites} between frequency bands). The coordination was generally weaker between more distant frequencies and absent or nearly absent for θ–β_2, θ–γ, and α–γ pairs. In addition, α, β_1, and β_2 bands tended to be somewhat jointly coordinated in the eyes-closed conditions, whereas the α–β_1 coordination tended to dissociate from the β_2–γ coordination (with diminished correlations for α–β_2 and β_1–β_2 pairs) in the eyes-open conditions.

Fig 13. Temporal correlations of n_{sites} (the number of concurrently activated/suppressed sites) between frequency bands. The correlations were computed as baseline-corrected Spearman's r, $\underline{r}_{sp}$ (r_{sp} minus baseline-r_{sp} computed based on phase-scrambled data) per frequency pair per participant per condition. **A–E.** Correlation matrices (symmetric about the diagonal) for spectral-power activations for the five behavioral conditions. Larger $\underline{r}_{sp}$ values are indicated with lighter colors. All $\underline{r}_{sp}$ values were statistically significant at $p<0.05$ (two-tailed, Bonferroni corrected). **F–J.** Line graphs comparing $\underline{r}_{sp}$ values among the cells labeled 1, 2, and 3 in A–E. The $\underline{r}_{sp}$ values were computed with Fisher-Z transformed r_{sp} and baseline- r_{sp} values to be appropriate for statistical comparisons. The thick lines with circular symbols indicate the means and the thin lines indicate the data from individual participants (all lines have been aligned at their respective means to highlight the variability in cell dependence). **K–O.** The same as A–E, but for spectral-power suppressions. The "-" symbols indicate statistically non-significant $\underline{r}_{sp}$ values. **P–T.** The same as F–J but for spectral-power suppressions.

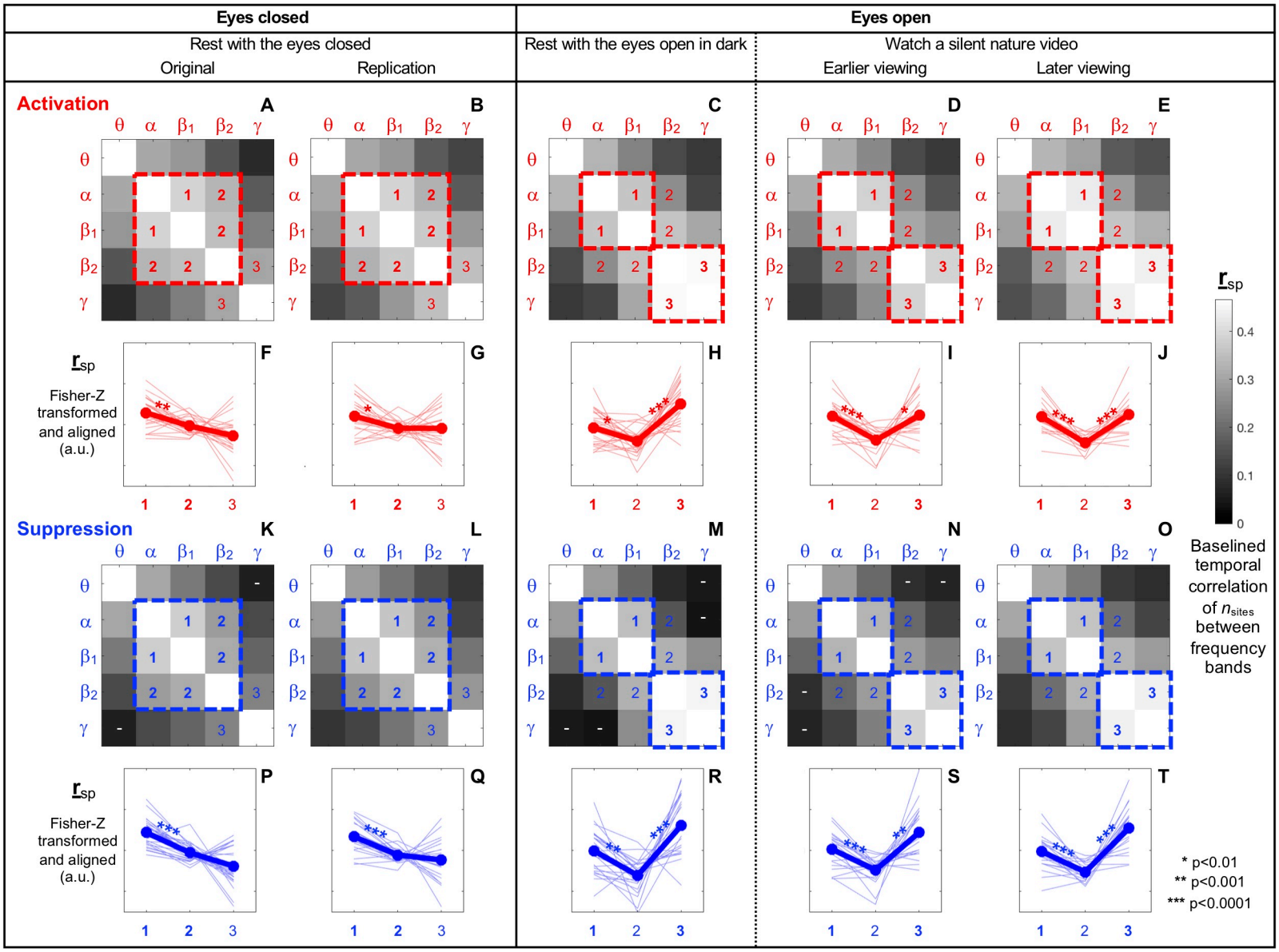
Eyes closed
Eyes open
Rest with the eyes closed
Original
Replication
Rest with the eyes open in dark
Watch a silent nature video
Earlier viewing
Later viewing
Activation
Suppression
A
B
C
D
E
F
G
H
I
J
K
L
M
N
O
P
Q
R
S
T
θ α β1 β2 γ
r̲sp
Fisher-Z transformed and aligned (a.u.)
r̲sp
0.4
0.3
0.2
0.1
0
Baselined temporal correlation of nsites between frequency bands
* p<0.01
** p<0.001
*** p<0.0001

Potential artifacts.

Might any of these results reflect artifacts? In particular, activities of the ocular muscles and the scalp muscles might have generated strong activations at specific scalp sites. While muscle artifacts tend to occur in the γ band [44–45], we observed characteristic small-scale and large-scale distributions of spectral-power activations in all representative frequency bands (Figures 3–7). Further, the fact that the average durations of small- and large-scale activations were prolonged (relative to the phase-scrambled controls) for all frequency bands by equivalent factors (Figure 2) is inconsistent with the possibility that γ band activations may have uniquely reflected muscle artifacts. The strongest evidence we have against any substantive contributions of muscle artifacts to our results is that the characteristic spatial distributions of activations and suppressions generally overlapped, especially for small-scale activations and suppressions and especially for γ band (Figures 3–7). Muscle artifacts would not generate consistent spatial distributions of spectral-power suppressions. The generally overlapping distributions of small-scale and large-scale activations and suppressions likely reflect activations and suppressions of the underlying small-scale and large-scale networks of neural sub-populations that tend to strongly synchronize and desynchronize concurrently.

Discussion

Oscillatory neural dynamics are prevalent in the brain [46], contributing to perceptual [16–17, 47–48], attentional [13, 20–22], memory [14], and cognitive [11–12,15,18] processes (and probably to many other processes), likely through controlling information flow by adjusting phase relations within and across frequency bands [3, 9–10, 21]. While phase relations are intricately coordinated across sub-populations depending on functional demands, an impact of phase realignments would be particularly high (or low) when the oscillatory activities within the relevant sub-populations are strongly synchronized (or desynchronized). We thus examined the spatiotemporal dynamics of maximal and minimal EEG spectral power, reflective of strongly synchronized and strongly desynchronized sub-populations. We set the thresholds for spectral-power activation and suppression to be the top and bottom 8% (per site per frequency band per condition per participant) that optimized the detection of isolated activations and suppressions (occurring exclusively at only one site) (Figure 1). The results yielded converging evidence suggesting that spectral-power activations and suppressions are organized into spatially segregated complementary networks, relatively isolated small-scale networks comprising only

1–4 (2%–7%) concurrently activated/suppressed sites and highly cooperative large-scale networks comprising 10+ (33+%) concurrently activated/suppressed sites.

First, instances of small-scale (involving 1–4 sites) and large-scale (involving 10+ sites), but not intermediate-scale (involving 5–9 sites), activations and suppressions were more prevalent and longer-lasting than expected from stochastic variations (Figure 2). This suggests that small-scale and large-scale activations and suppressions are actively maintained. Second, small-scale and large-scale (but not intermediate-scale) activations and suppressions consistently segregated in specific regions with generally overlapping distributions for activations and suppressions (Figures 3–7). This suggests that strong synchronizations and desynchronizations occur in spatially segregated small-scale and large-scale networks. Third, the characteristic spatial patterns of spectral-power activations and suppressions were generally stable while activations/suppressions fluctuated within the small-scale or large-scale (but not intermediate-scale) range (Figures 8–12). Some of the characteristic large-scale, but not small-scale, spatial patterns of activations were observed during extensive expansions and contractions of activations, but none of the characteristic patterns of suppressions were observed during extensive expansions or contractions of suppressions. These contextual dependences suggest that the characteristic small-scale and large-scale spatial patterns of activations/suppressions primarily emerge and dissolve while activations/suppressions remain within the small-scale or large-scale range.

Taken together, these results suggest that the spatiotemporal dynamics of maximal and minimal spectral power, that is, the spatiotemporal dynamics of strong synchronizations and desynchronizations of oscillatory neural activities in the sub-populations reflected in EEG current sources, are characterized by spatially segregated small-scale networks where sub-populations are strongly synchronized or desynchronized in relative isolation and large-scale networks where the sub-populations are strongly synchronized or desynchronized in a highly cooperative manner. These small-scale and large-scale networks of concurrently synchronized/desynchronized sub-populations likely confer an overarching dynamic structure that constrains the impact of demand-based realignments of phase relations within and across frequency bands and brain regions. Future research may investigate how phase-relation realignments are coordinated with the status (strongly synchronized or desynchronized) of these small- and large-scale synchronization networks to optimize information processing.

Our results also suggest that these networks are frequency specific (Figures 3–7 and Figures 8–12). Although speculating on the relationships between the frequency-specific networks identified here and the numerous examples of task-dependent oscillatory activities

reported in the literature is beyond the scope of the current discussion, we summarize some notable features of the identified frequency-specific synchronization networks. First, in the eyes-closed condition, the small-scale networks for the θ, α, β_1, and β_2 bands all included the frontal region, while the large-scale networks systematically shifted from including primarily posterior regions for the θ band, posterior and medial-anterior regions for the α band, posterior and lateral-anterior regions for the β_1 band, primarily lateral-anterior regions for the β_2 band, and consistently lateral-anterior regions for the γ band (Figures 3–7, parts A and B). Second, regardless of behavioral condition, the small-scale networks were consistently localized in the medial-central-posterior regions and the large-scale networks were localized in the lateral-anterior regions for the γ band (Figure 7). Third, the networks for the β_2 band in the eyes-open conditions (eyes open in dark and watching a nature video) clustered nearly identically to the networks for the γ band (Figure 6C–6F and Figure 7A–7F). Further, the temporal coordination of small- and large-scale networks (in terms of the temporal correlations of n_{sites} for both activations and suppressions) was uniquely elevated between β_2 and γ bands in the eyes-open conditions (Figure 13, parts C–E and M–O), suggestive of close spatiotemporal coordination of synchronization and desynchronization between β_2 and γ bands unique to the state of the eyes being open (regardless of visual stimulation). Overall, the networks were only modestly coordinated ($\underline{r}_{sp} < 0.5$) across frequency bands, primarily between proximate frequency bands, but virtually uncoordinated between distant bands (Figure 13, parts A–E and K–O).

To conclude, many studies have examined the spatiotemporal dynamics of spectral-power and phase relations to identify a variety of within- and cross-frequency interactions of oscillatory activities contributing to various behavioral functions (see citations above). What is unique about the current study is the examination of spontaneous spatiotemporal dynamics of maximal and minimal spectral-power activities focusing on their spatial scale. In this way, we were able to determine that strong synchronizations and desynchronizations occur in complementary small-scale and large-scale networks that are spatially segregated and frequency specific, thus segregating the relatively independent and highly cooperative oscillatory processes.

References

1. Osipova, D., Hermes, D., & Jensen, O. (2008). Gamma-power is phase-locked to posterior alpha activity. *PLoS ONE, 3(12), e3990*, 1-7.

2. Hipp, J. F., Hawellek, D. J., Corbetta, M., Siegel, M., & Engel, A. K. (2012). Large-scale cortical correlation structure of spontaneous oscillatory activity. *Nature Neuroscience, 15(6)*, 884-890.

3. Palva, S., & Palva, J. M. (2012). Discovering oscillatory interaction networks with M/EEG: challenges and breakthroughs. *Trends in Cognitive Sciences, 16(4)*, 219-230.

4. Spaak, E., Bonnefond, M., Maier, A., Leopold, D. A., & Jensen, O. (2012). Layer-specific entrainment of gamma-band neural activity by the alpha rhythm in monkey visual cortex. *Current Biology, 22(24)*, 2313–2318.

5. Michalareas, G., Vezoli, J., van Pelt, S., Schoffelen, J.-M., Kennedy, H., & Fries, P. (2016). Alpha-beta and gamma rhythms subserve feedback and feedforward influences among human visual cortical areas. *Neuron, 89*, 384-397.

6. Müller, V., Perdikis, D., Oertzen, T., Sleimen-Malkoun, R, Jirsa, V., & Lindenberger, U. (2016). Structure and topology dynamics of hyper-frequency networks during rest and auditory oddball performance. *Frontiers in Computational Neuroscience, 10, Article 108*, 1-25.

7. Olejarczyk, E., Marzetti, L., Pizzella, V., & and Zappasodi, F. (2017). Comparison of connectivity analyses for resting state EEG data. *Journal of Neural Engineering, 14, 036017*, 1-13.

8. Stankovski, T., Ticcinelli, V., McClintock, P. V. E., & Stefanovska, A. (2017). Neural cross-frequency coupling functions. *Frontiers in Systems Neuroscience, 11, Article 33*, 1-13.

9. Rubinov, M., & Sporns, O. (2010). Complex network measures of brain connectivity: uses and interpretations. *NeuroImage*, 52, 1059-1069.

10. Fries, P. (2005). A mechanism for cognitive dynamics: neural communication through neural coherence. *Trends in Cognitive Sciences, 9(10)*, 474-480.

11. Palva, J. M., Palva, S., & Kaila, K. (2005). Phase synchrony among neuronal oscillations in the human cortex. *Journal of Neuroscience, 25(15)*, 3962-3972.

12. Palva, S., & Palva, M. (2007). New vistas for α-frequency band oscillations. *Trends in Neurosciences, 30(4)*, 150-158.

13. Busch, N. A., & VanRullen, R. (2010). Spontaneous EEG oscillations reveal periodic sampling of visual attention. *Proceedings of the National Academy of Sciences, 107(37)*, 16048-16053.

14. Duzel, E., Penny, W. D., & Burgess, N. (2010). Brain oscillations and memory. *Current Opinion in Neurobiology, 20*, 143-149.

15. Engel, A. K., & Fries, P. (2010). Beta-band oscillations—signaling the status quo? *Current Opinion in Neurobiology, 20*, 156-165.

16. Voytek, B., Canolty, R. T., Shestyuk, A., Crone, N. E., Parvizi, J., & Knight, R. T. (2010). Shifts in gamma phase-amplitude coupling frequency from theta to alpha over posterior cortex during visual tasks. *Frontiers in Human Neuroscience, 4*, A191, 1-9.

17. Dehaene, S., & Changeux, J.-P. (2011). Experimental and theoretical approaches to conscious processing. *Neuron, 70*, 200-227.

18. Donner, T. H., & Siegel, M. (2011). A framework for local cortical oscillation patterns. *Trends in Cognitive Sciences, 15(5)*, 191-199.

19. Arnal, L.H., Giraud, A.L. (2012). Cortical oscillations and sensory predictions. *Trends in Cognitive Sciences, 16 (7)*, 390-398.

20. Klimesch, W. (2012). Alpha-band oscillations, attention, and controlled access to stored information. *Trends in Cognitive Sciences, 16(12)*, 606-617.

21. Jensen, O., Gips, B., Bergmann, T. O., & Bonnefond, M. (2014). Temporal coding organized by coupled alpha and gamma oscillations prioritize visual processing. *Trends in Neurosciences, 37(7)*, 357-369.

22. Bonnefond, M, & Jensen, O. (2015). Gamma activity coupled to alpha phase as a mechanism for top-down controlled gating. *PLoS ONE, 10(6)*: e0128667, 1-11.

23. Adebimpe, A., Arabi, A., Bourel-Ponchel, E., Mahmoudzadeh, M., & Wallois, F. (2016). EEG resting state functional connectivity analysis in children with benign epilepsy with centrotemporal spikes. *Frontiers in Neuroscience, 10, Article 143*, 1-9.

24. Antonakakis, M., Dimitriadis, S. I., Zervakis, M., Micheloyannis, S., Resaie, R., Babajani-Feremi, A., Zouridakis, G., & Papanicolaou, A. C. (2016). Altered cross-frequency coupling in resting-state MEG after mild traumatic brain injury. *International Journal of Psychophysiology, 102*, 1-11.

25. Gonzalez, G. F., Simt, D. J. A., van der Molen, M. J. W., Tijms, J., Stam, C. J., de Geus, E. J. C., & van der Molen, M. W. (2018). EEG resting state functional connectivity in adult dyslexics using phase lag index and graph analysis. *Frontiers in Human Neuroscience, 12, Article 341*, 1-12.

26. Scally, B., Burke, M. R., Bunce, D., & Delvenne, J.-F. (2018). Resting-state EEG power and connectivity are associated with alpha peak frequency slowing in healthy aging. *Neurology of Aging, 71*, 149-155.

27. Menceloglu, M., Grabowecky, M., & Suzuki, S. (under review). Probabilistic, entropy maximizing control of large-scale neural synchronization. https://www.biorxiv.org/content/10.1101/2020.08.09.243295v1

28. Delorme, A., & Makeig, S. (2004). EEGLAB: an open source toolbox for analysis of single-trial EEG dynamics including independent component analysis. *Journal of neuroscience methods*, *134*(1), 9-21.

29. Lopez-Calderon, J., & Luck, S. J. (2014). ERPLAB: an open-source toolbox for the analysis of event-related potentials. *Frontiers in human neuroscience*, *8*, 213.

30. Makeig, S., Bell, A. J., Jung, T.-P. and Sejnowski, T. J. (1996). "Independent component analysis of electroencephalographic data," In: D. Touretzky, M. Mozer and M. Hasselmo (Eds). Advances in Neural Information Processing Systems 8:145-151, MIT Press, Cambridge, MA.

31. Makeig, Scott et al. "EEGLAB: ICA Toolbox for Psychophysiological Research". WWW Site, Swartz Center for Computational Neuroscience, Institute of Neural Computation, University of San Diego California <www.sccn.ucsd.edu/eeglab/>, 2000. [World Wide Web Publication].

32. Cohen, M. X. (2014). *Analyzing Neural Time Series Data: Theory and Practice*, MIT Press.

33. Hjorth, B. (1980). Source derivation simplifies topographical EEG interpretation. *American Journal of EEG Technology 20*, 121-132.

34. Kayser, J., Tenke, C. E. (2006). Principal components analysis of Laplacian waveforms as a generic method for identifying ERP generator patterns: I. Evaluation with auditory oddball tasks. *Clinical Neurophysiology, 117*, 348-368.

35. Tenke, C. E., & Kayser, J. (2012). Generator localization by current source density (CSD): Implications of volume conduction and field closure at intracranial and scalp resolutions. *Clinical Neurophysiology, 123*, 2328–2345.

36. Perrin, F., Pernier, J., Bertrand, O., Giard, M. H., & Echallier, J. F. (1987). Mapping of Scalp Potentials by Surface Spline Interpolation. *Electroencephalography and Clinical Neurophysiology, 66 (1)*, 75-81.

37. Perrin, F., Pernier, J., Bertrand, O., & Echallier, J. F. (1989). Spherical Splines for Scalp Potential and Current Density Mapping. *Electroencephalography and Clinical Neurophysiology 72(2)*: 184-187.

38. Perrin, F., Pernier, J., Bertrand, O., & Echallier, J. F. (1989). Corrigenda EEG 02274. *Electroencephalography and Clinical Neurophysiology 76*, 565.

39. Menceloglu, M., Grabowecky, M., & Suzuki, S. (2020). Spectral-power associations reflect amplitude modulation and within-frequency interactions on the sub-second timescale and cross-frequency interactions on the seconds timescale. *PLoS ONE*, 15(5): e0228365.

40. Menceloglu, M., Grabowecky, M., & Suzuki, S. (2020). EEG state-trajectory instability and speed reveal global rules of intrinsic spatiotemporal neural dynamics. *PLoS ONE*. 15(8): e0235744.

41. Kiya, H., Ito, I., & Miron, S. (2010). "Phase scrambling for image matching in the scrambled domain" in Signal Processing, *InTech*, 97-414.

42. Hess, R. F. & Snowden, R. J., (1992) Temporal properties of human visual filters: Number, shapes and spatial covariance, *Vision Research, 32*, 47-60.

43. Lui, L. L., Bourne, J. A., Rosa, M. G. P. (2007). Spatial and temporal frequency selectivity of neurons in the middle temporal visual area of new world monkeys (Callithrix jacchus). *European Journal of Neuroscience, 25*, 1780-1792.

44. Hipp, J. F., & Siegel, M. (2013). Dissociating neuronal gamma-band activity from cranial and ocular muscle activity in EEG. *Frontiers in Human Neuroscience, 7: 338*. doi: 10.3389/fnhum.2013.00338

45. Muthukumaraswamy, S. D. (2013). High-frequency brain activity and muscle artifacts in MEG/EEG: a review and recommendations. *Frontiers in Human Neuroscience, 7: 138*. doi: 10.3389/fnhum.2013.00138

46. Buzsaki, G. (2006). *Rhythms of the Brain*, Oxford University Press.

47. Mathewson, K. E., Gratton, G., Fabiani, M., Beck, D. M., & Ro, T. (2010). To see or not to see: prestimulus alpha phase predicts visual awareness. *Journal of Neuroscience, 29*, 2725-2732.

48. Mathewson, K. E., Lleras, A., Beck, D. M., Fabiani, M., Ro, T., Gratton, G. (2011). Pulsed out of awareness. EEG alpha oscillations represent a pulsed-inhibition of ongoing cortical processing. *Frontiers in Psychology, 2, A99*, 1-15.

49. Menceloglu, M., Grabowecky, M., & Suzuki, S. (2020). Spectral-power associations reflect amplitude modulation and within-frequency interactions on the sub-second timescale and cross-frequency interactions on the seconds timescale. *PLoS ONE*, 15(5): e0228365. https://doi.org/10.1371/journal.pone.0228365

50. Menceloglu, M., Grabowecky, M., & Suzuki, S. (2020). EEG state-trajectory instability and speed reveal global rules of intrinsic spatiotemporal neural dynamics. *PLoS ONE*. 15(8): e0235744. https://doi.org/10.1371/journal.pone.0235744